Contrast gain control: a bilinear model for chromatic selectivity

Benjamin Singer and Michael D'Zmura

Department of Cognitive Sciences and Institute for Mathematical Behavioral Sciences, University of California, Irvine, Irvine, California 92717

Received July 22, 1994; revised manuscript received November 3, 1994; accepted November 3, 1994

We report the results of psychophysical experiments on color contrast induction. In earlier work [Vision Res. **34,** 3111 (1994)], we showed that modulating the spatial contrast of an annulus in time induces an apparent modulation of the contrast of a central disk, at isoluminance. Here we vary the chromatic properties of disk and annulus systematically in a study of the interactions among the luminance and the color-opponent channels. Results show that induced contrast depends linearly on both disk and annulus contrast, at low and moderate contrast levels. This dependence leads us to propose a bilinear model for color contrast gain control. The model predicts the magnitude and the chromatic properties of induced contrast. In agreement with experimental results, the model displays chromatic selectivity in contrast gain control and a negligible effect of contrast modulation at isoluminance on the appearance of achromatic contrast. We show that the bilinear model for chromatic selectivity may be realized as a feed-forward multiplicative gain control. Data collected at high contrast levels are fit by embellishing the model with saturating nonlinearities in the contrast gain control of each color channel.

Key words: color, contrast, contrast gain control, color appearance, color constancy, luminance and chromatic channels, contrast adaptation, cardinal color directions, color–luminance interactions.

1. INTRODUCTION

The color appearance of a central area is influenced by the chromatic properties of lights from surrounding areas. This influence is demonstrated in studies of simultaneous contrast[1,2] and in studies of color constancy.[4] While much earlier work has concerned the way that the space-averaged light from surrounding areas affects central appearance, recent attention has focused on the effects of variability among surrounding lights.[5–8]

We investigated the effects of varying the contrast in surrounding areas in experiments on contrast gain control.[3] Fast-acting mechanisms for contrast gain control had been revealed earlier by Chubb *et al.*[9] in psychophysical experiments with achromatic stimuli. Using patterned stimuli similar to those of Chubb and colleagues, we showed that modulating the contrast of an annular surround induces an apparent modulation of the contrast of a central disk, at isoluminance. We studied this contrast induction, using disks and annuli that presented spatial contrast along the achromatic (A), the long- and-middle-wavelength-sensitive- (L&M-) or the short-wavelength-sensitive- (S-) cone axes of color space.[10–12] Apparent contrast induction was measured with a nulling technique.[9,13]

We established that contrast gain control mechanisms are binocular.[3] An apparent modulation of disk contrast is readily observable when disk and annulus are presented steadily to different eyes and the contrast of the annulus is modulated in time. We found interocular transfer using both achromatic stimuli and isoluminant stimuli along the L&M-cone or the S-cone axis. This positive result with steadily presented stimuli contrasts with the lack of interocular transfer reported by Chubb and colleagues[9] and by Solomon *et al.*,[14] who used briefly flashed stimuli. We also found that the temporal-frequency cutoff of the mechanisms responsible for contrast gain control is rather low, at ~8 Hz. Modulating the annulus contrast at rates above this frequency causes no visible alterations in disk contrast. Low-pass temporal-frequency sensitivities with cutoff frequencies of 8 Hz were found for both achromatic and isoluminant stimuli. We also determined that modulating contrast within a circular area of diameter 4 deg of visual angle produces an effect that is little increased if the area increases in size. We found this contrast pooling area, determined for foveal viewing, using both achromatic and isoluminant stimuli. These three results suggest a cortical locus for contrast gain control: receptive fields are large, sluggish, and binocular.[3]

We also showed that contrast gain control is chromatically selective: contrast modulation along one axis in color space affects apparent contrast more strongly along the same axis than along a different axis.[3] This selectivity is similar to that found by Webster and Mollon in their extensive studies of how habituation to chromatic modulation affects color appearance.[15,16] Chromatic selectivity is analogous to the spatial-frequency selectivity and to the orientation selectivity found previously for contrast gain control.[9,14,17]

In an attempt to understand and model the chromatic selectivity of contrast gain control, we were guided by two results of our earlier study.[3] First, the strength of induced modulation depends approximately linearly on the size of the modulation of annulus contrast, for low to moderate contrast modulations. Second, the size of the induced modulation depends approximately linearly on the contrast of the central disk. We obtained both results using disks and annuli with identical chromatic properties.

0740-3232/95/040667-19$06.00

These results suggest a bilinear model for the chromatic properties of contrast gain control. Bilinear models have been used previously to model the effects of moderate chromatic adaptation on color appearance.[18–20] They have also been used in work on computational color constancy.[21–25]

In this paper we first present methods and results of experiments that test whether contrast induction depends linearly on both central and surrounding area contrast. We find that these linearities hold for low- and moderate-contrast stimuli in the three dimensions of color space. On the strength of the results, we present a bilinear model for predicting the apparent chromatic modulation of a central area that is induced by modulating the contrast of a surrounding area. In agreement with the results of psychophysical experiments, the model displays chromatic selectivity and a negligible effect of isoluminant contrast modulation on achromatic appearance.

We then examine experimentally the effects of varying the average contrast of the annulus and compare the results with model predictions. Bilinear model predictions describe results at low annulus contrasts well but fail at high annulus contrasts, where contrast induction is reduced in a way that suggests the operation of saturating nonlinearities. To help understand the nonlinearities, we present a realization of the bilinear model as a feed-forward matrix-multiplicative gain control. The multiplicative form of the proposed gain control, which contrasts with the divisive form used in other models, such as those of Sperling[26] and Heeger,[27] is a natural consequence of bilinearity. We include saturating nonlinearities in the contrast gain control of each color channel to fit data at high contrasts. This research was reported in preliminary form elsewhere.[28]

2. METHODS

The stimuli are similar to those used in our earlier work.[3] We modulated in time the contrast of an annulus containing spatial noise and used a nulling technique to measure the induced contrast modulation of a central disk.

Stimuli were presented on a Sony Trinitron GDM-1960 color monitor that was viewed binocularly at a distance of 1 m. We used a DECstation 5000/200 computer to control a Turbo PXG+ graphics board, which provided a 1280×1024 pixel display at a rate of 66 Hz (noninterlaced). The spectra, chromaticities, and luminances of the monitor's three phosphors were measured with a Photo Research PR-650 SpectraColorimeter. By means of color lookup tables we used these measurements to correct for the nonlinear relationship between applied voltage and phosphor intensity. The screen was set to display a steady, gray background of luminance 51 cd/m^2 and chromaticity (0.28, 0.30) for the CIE 1931 standard observer.

Stimulus spatial properties are shown in Fig. 1. We used a 512-pixel-diameter disk–annulus stimulus comprising spatially isotropic binary noise. The diameters of the disk and of the annulus were 2 and 8 deg of visual angle, respectively. We computed binary noise patterns by (1) calculating a spatially isotropic difference-of-Gaussians amplitude spectrum, in which the two Gaussians had identical peak values and had spatial standard deviations of 0.625 and 1.875 deg of visual angle; (2) creating a random phase spectrum; (3) applying an inverse Fourier transform to the spectra to provide noise in the space domain, and (4) binarizing the result to make spatially isotropic binary noise with a peak in its spatial frequency power spectrum at ~1.8 cycle/deg.

We modulated the chromatic properties of the disk and the annulus independently by rewriting color lookup table entries. We describe these chromatic properties in a color space based on the cardinal axes of Krauskopf and his colleagues.[11,12,29] An isoluminant plane passes through a white point W that represents the neutral background in these experiments. The plane is determined photometrically and is spanned by two cardinal axes. The first of these is the L&M-cone axis, modulations along which are visible only to the long- and medium-wavelength-sensitive cones. The second is the S-cone axis, modulations along which are visible only to the short-wavelength-sensitive cones. We use the Smith–Pokorny[10] spectral sensitivity functions to determine these axes. Lights along the L&M-cone axis appear red or blue-green, and lights along the S-cone axis appear yellow-greeen or purple. An achromatic axis completes the color space.

Calculations using the Smith–Pokorny[10] fundamentals and measurements using the spectroradiometer show that the maximum contrast available along the L&M-cone axis was 8.2% to L cones. The maximum contrast available along the S-cone axis was 86% to S cones.

Both disk and annulus contained binary noise and so presented two (generally distinct) lights at any one time. We varied the annulus lights in time to modulate contrast while leaving unchanged the space-averaged light. The two regions of the annulus were assigned complementary chromaticities along a color-space axis through the white point. As a result, the space-averaged light from the an-

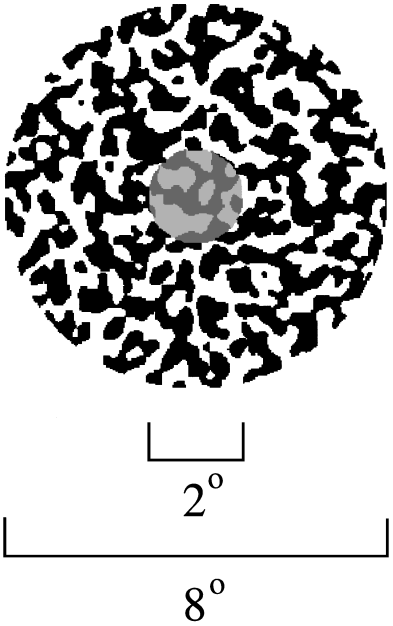

Fig. 1. Stimulus spatial properties. A central disk with a diameter of 2 deg of visual angle and an annulus with a diameter of 8 deg were filled with binary noise. The stimulus was centered on a gray rectangular background that was 16 deg high by 20 deg wide. See text for further details.

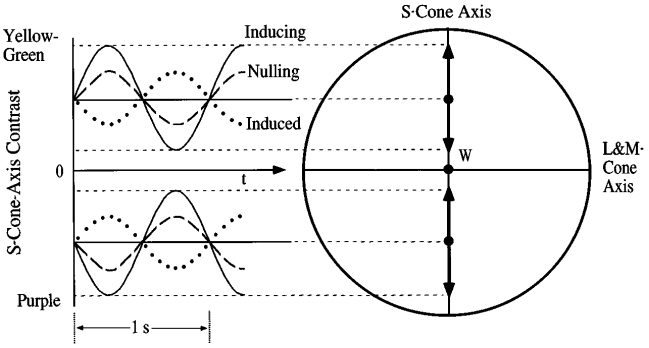

Fig. 2. Stimulus chromatic properties. At left is depicted the time-varying contrast modulation of an annulus at 1 Hz (solid curves, Inducing) with mean contrast and contrast modulation along the S-cone axis. The dotted curves (Induced) depict the induced modulation in the appearance of a physically steady central disk, also with chromaticities along the S-cone axis. The dashed curves (Nulling) indicate the physical modulation of disk contrast that is needed to make the disk appear steady.

nulus was equivalent to the gray background. Figure 2 describes the situation in which the annulus has yellow-green and purple regions with chromaticities drawn from the S-cone axis. The two annulus lights were modulated sinusoidally in counterphase about their mean values to produce a contrast modulation along a color-space axis identical to that along which lay the means.

The central disk comprised binary noise with lights bearing complementary chromaticities. When the two lights from the disk were held steady, it was often the case that modulating the annulus contrast induced an apparent contrast modulation of the central disk in counterphase (see Fig. 2). At isoluminance such changes in disk contrast appeared as modulations of color saturation. As described in the earlier paper,[3] we made photometric measurements that confirmed that annulus contrast could be varied independently of disk physical properties.

Following Krauskopf and colleagues[13] and Chubb and colleagues,[9] we asked observers to determine the amplitude of the nulling modulation that, when added to the disk, would remove any apparent modulation of disk contrast (see Fig. 2). We used the method of constant stimuli. We presented each observer different amplitudes of disk contrast modulation in an effort to determine the nulling contrast modulation. We controlled with software the color-space axes and contrasts of the annulus mean, the annulus contrast modulation, the disk mean, and the disk contrast modulation.

The disk stimulus is described by a space- and time-varying color vector $\mathbf{D}(\mathbf{x}, t)$. This three-dimensional vector in color space is a linear combination of the white point vector $\mathbf{w}$ (the neutral gray background), the disk mean contrast vector $\mathbf{d}$, and the disk contrast-modulation vector $\boldsymbol{\delta}$:

$$\mathbf{D}(\mathbf{x}, t) = \mathbf{w} + b_D(\mathbf{x})[\mathbf{d} + \boldsymbol{\delta} \sin(2\pi t)], \quad (1)$$

in which $b_D(\mathbf{x})$ describes the spatial dependence of the disk binary noise pattern and takes on values ± 1 within the disk area and 0 elsewhere and $\sin 2\pi t$ represents the temporal modulation of contrast at 1 Hz. Likewise, the annulus stimulus $\mathbf{A}(\mathbf{x}, t)$ is described by the following sum:

$$\mathbf{A}(\mathbf{x}, t) = \mathbf{w} + b_A(\mathbf{x})[\mathbf{a}_m + \boldsymbol{\alpha} \sin(2\pi t)], \quad (2)$$

in which $b_A(\mathbf{x})$ describes the annulus binary noise, $\mathbf{a}_m$ is the annulus mean contrast vector, and $\boldsymbol{\alpha}$ is the annulus contrast-modulation color vector. The task of the observers was to determine the value of disk contrast modulation that would best null the induced modulation.

Observers adapted to the steady gray background for 1 min at the beginning of each run. Each trial started with the appearance of a cross hair at the display's center, where the center of the stimulus would later appear. The observer then indicated readiness for the stimulus with a key press. The cross hair disappeared, and two beeps sounded. After a delay of 1 s, the disk–annulus stimulus appeared. Observers were instructed to maintain fixation at the center of the disk. Two cycles of annulus and disk contrast modulation at 1 Hz followed; the stimulus then disappeared, leaving the neutral background.

Observers were forced to choose whether disk contrast appeared to modulate in phase or in counterphase with the annulus contrast modulation. Each such choice was represented by three possible levels of confidence, so creating six possible choices ranging from definitely in phase to definitely in counterphase. Disk contrast-modulation levels were chosen to span the response range. The midpoint of this response range represents cases in which the disk contrast modulation nulls the apparent modulation induced by the modulation of the annulus contrast. Observers were instructed to respond as rapidly as possible. A pause of 5 s followed each response, before the self-presentation of the next trial.

The number of trials per condition varied by experiment. In general, trials that presented different levels of the independent variable were interspersed randomly, and for each of these levels a number of disk contrast modulations were presented repeatedly, as in the method of constant stimuli. For instance, each of the nine chromatic conditions in the experiment on the effects of annulus contrast modulation (Subsection 3.A) involved 250 trials per observer. Five levels of annulus contrast modulation were presented, and for each of these levels ten disk contrast modulations were presented five times apiece. In later experiments each condition comprised 150 trials: six rather than ten disk contrast modulations were presented.

The confidence judgments found at each level describe psychometric functions that were fitted by sigmoids to help estimate at what disk contrast modulation the responses change from in phase to in counterphase. We found the horizontal position and the steepness of the sigmoids by using the minimization function `fmins` in `MATLAB` (The Mathworks, Inc.).

Three observers participated in the experiments, including author BS and two naïve observers, JC and JL. Two additional naïve observers, JH and LD, participated in a subset of experiments. All observers had normal color vision as tested with Ishihara plates[30] and were properly refracted.

3. RESULTS ON LINEAR DEPENDENCIES

The two most important components of the bilinear model that we present below are the linear dependencies of induced contrast on central and surrounding area contrasts. Are these dependencies, in fact, linear? The fol-

lowing experiments test for these linearities in the three dimensions of color space. The experiments probe the dependencies in the (general) case in which central and surrounding areas have different chromatic properties. Note that with the nulling technique we measure the dependencies of induced contrast on central contrast and on the *modulation* of surrounding area contrast. Our particular aim was to test for linearity at low and moderate contrast levels, as earlier research had shown that induced modulation saturates at high levels of contrast.[3]

A. Dependence on Annulus Contrast Modulation

We first examined whether the contrast modulation needed to null induced modulation increases linearly as annulus contrast modulation increases. We chose annulus lights to lie along the achromatic, the L&M-cone, or the S-cone axis in an experimental condition. The mean annulus contrast was set to 30% of the maximum displayable contrast along each axis. These contrast levels were chosen to avoid saturating nonlinearities of the sort found in earlier research.[3] As described in Section 2, these maximum contrasts were 100% along the achromatic axis, 8.2% to L cones along the L&M-cone axis, and 86% to S cones along the S-cone axis. In an experimental condition the amplitude of the annulus contrast modulation was varied from 10% to 30% of the maximum displayable contrast in 5% steps.

The central disk lights were chosen from the lights along the achromatic, the L&M-cone, or the S-cone axis. There were thus nine possible color combinations: three color axes for the annulus by three color axes for the disk. Disk mean contrast was set to 30% of the maximum displayable contrast. On a given trial the observer was presented a disk contrast modulation drawn from a range of values that spanned the modulation that would null the induced modulation.

The disk contrast modulations were always presented along the disk axis, and this restriction in the choice of nulling modulation reflects an important result: when disk chromatic properties are restricted to lie along one of the three cardinal axes in the color space, induced modulation takes the form of a modulation of either contrast (for the achromatic axis) or color saturation (for the L&M-cone and the S-cone axes). One can null induced effects by modulating disk contrast along the cardinal color axis of the disk.[3]

The nulling modulations that were measured for each of the nine color-axis combinations for disk and annulus are shown in the nine panels of Fig. 3. The color-space axis of the annulus varies from left to right. Results in the left column pertain to achromatic annuli, in the middle column to annuli along the L&M-cone axis, and in the right column to annuli along the S-cone axis. The color space axis of the disk varies from top to bottom. Results in the top, middle, and bottom rows are for achromatic, L&M-cone-, and S-cone-axis disks, respectively.

The data points show the nulling modulations averaged across three observers; error bars show estimates of the standard error of the mean. The amplitude of annulus contrast modulation varies along the horizontal axis of each plot in units specific to the cardinal axis of the annulus. These units are not maximum displayable contrast units; rather, they are units of contrast to cone mechanisms. For achromatic-axis stimuli contrast is scaled in the standard way, whereas for L&M-cone-axis stimuli and for S-cone-axis stimuli the contrast scales describe contrast to L cones and to S cones, respectively. The amplitude of disk contrast modulation that is needed to null the induced apparent modulation of the disk varies along the vertical axis of each plot. Again, contrast units along vertical axes are specific to the color-space axis of the disk.

We fitted lines to the data, using slope as the only parameter (see Table 1). In four cases (achromatic disks with achromatic annuli in Fig. 3A and S-cone disks in Figs. 3G, 3H, and 3I), apparent response saturation occurred in the tested range, and the affected data were excluded from the fits. The excluded points are shown in Fig. 3 as open circles. Lines fit the remaining data excellently. At least 98% of the variance was accounted for in all the fits, and in most cases more than 99% was accounted for (see Table 1).

Agreement among observers was excellent; all their results displayed a pattern that agrees with the results of our earlier experiment on chromatic selectivity.[3] First, contrast induction is strongest when disk and annulus share the same cardinal axis (Figs. 3A, 3E, and 3I). Second, annulus contrast modulation at isoluminance has a negligible effect on the appearance of achromatic contrast (Figs. 3B and 3C).

The linear fits show that induced modulation of contrast in a central disk depends approximately linearly on the contrast modulation of a surrounding annulus. The results suggest that this holds true in a linear range of small to moderate contrast levels in three-dimensional color space, in cases in which disk and annulus have different chromatic properties.

B. Dependence on Disk Mean Contrast

We tested second whether nulling contrast modulations increase linearly as disk mean contrast increases. Both the annulus mean contrast and the annulus contrast modulation were held fixed at 30% and 20%, respectively, of the maximum displayable contrasts along their respective axes. Again, we chose these modest contrast levels to avoid saturating nonlinearities.

Each experimental condition corresponded to a particular choice of one of the nine possible combinations of cardinal axes for disk and annulus. Disk mean contrast on a particular trial was chosen randomly from the range 10–30%, represented at 5% steps, of the maximum displayable contrast. A disk contrast modulation was drawn from a range of values that spanned the nulling modulation on a given trial. Again, these disk contrast modulations were always presented along the color space axis of the disk.

The results are shown in Fig. 4. The color-space axis of the disk varies from left to right; results in the left, middle, and right columns are for achromatic, L&M-cone-, and S-cone-axis disks, respectively. The color-space axis of the annulus varies from top to bottom; the top, middle, and bottom rows hold results for achromatic, L&M-cone-, and S-cone-axis annuli, respectively. The amplitude of disk mean contrast varies along the horizontal axis of each plot in units specific to the color-space axis, and the amplitude of nulling modulation varies along each plot's vertical axis.

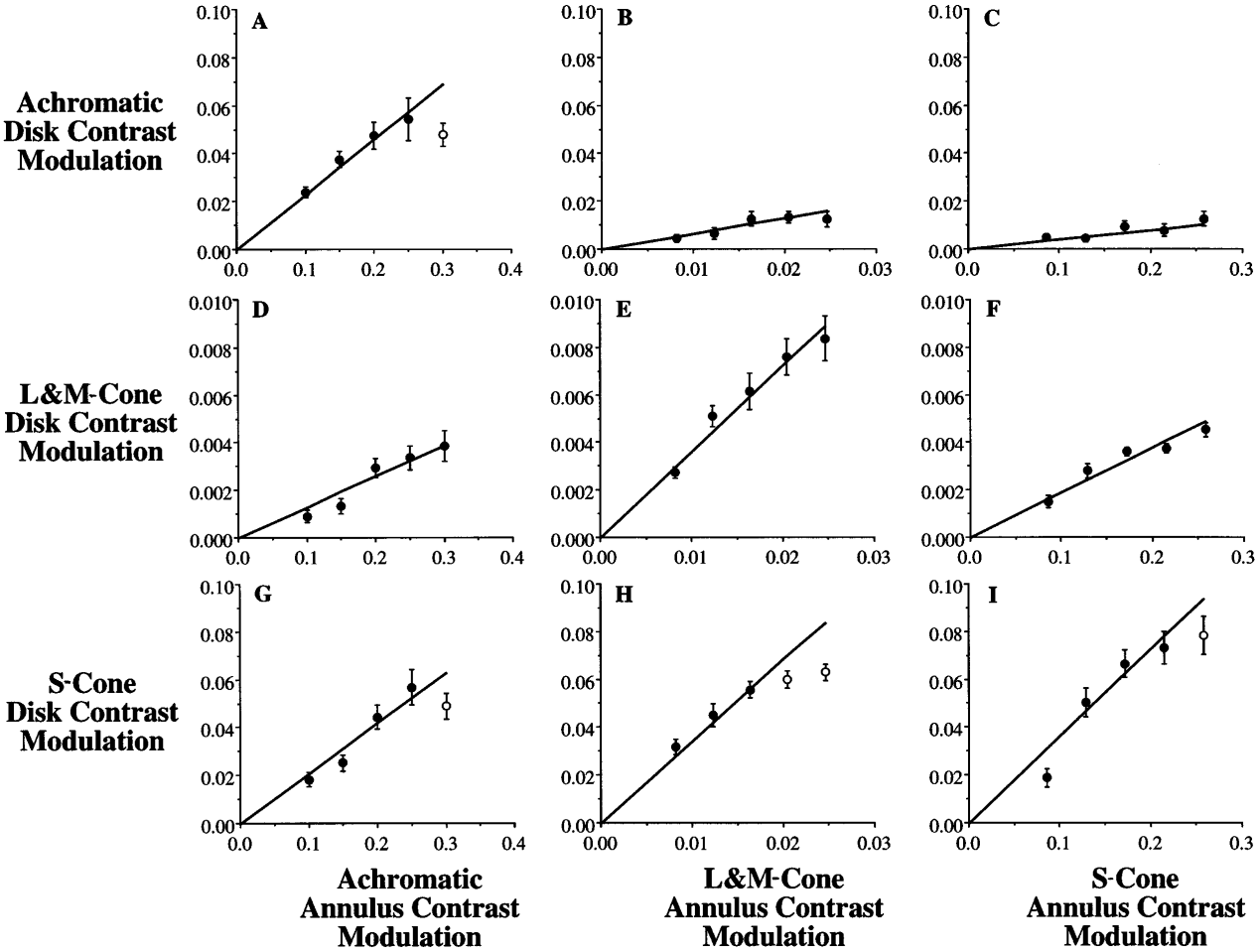

Fig. 3. Dependence of contrast induction on annulus contrast modulation. Panels in the left, middle, and right columns describe results with annuli along the achromatic, L&M-cone, and S-cone axes, respectively. Panels in the top, middle, and bottom rows describe results with disks along the achromatic, L&M-cone, and S-cone axes, respectively. Along each horizontal axis varies the amplitude of the annulus contrast modulation. Along each vertical axis varies the amplitude of the disk contrast modulation that is needed to null the induced modulation. Units of measurement are specific to each axis: we use standard contrast units along the achromatic axis, contrast to L cones along the L&M-cone axis, and contrast to S cones along the S-cone axis. Each data point represents results averaged across the three observers JC, JL, and BS; error bars represent estimates of the standard error of the mean. Lines are fitted to the data with slope as the only parameter. Data points marked by open circles are excluded from the fits. See text for details.

Table 1. Slopes of Lines Fitted to the Data in Fig. 3 and Goodness of Fit for the Average of the Observers

Condition (Disk, Annulus)	Slope	R^2
A, A	0.229	0.995
L&M, A	0.012	0.999
S, A	0.206	0.992
A, L&M	0.653	0.997
L&M, L&M	0.362	0.999
S, L&M	3.423	0.996
A, S	0.044	0.997
L&M, S	0.017	0.999
S, S	0.363	0.986

The data points show averages for three observers. We fitted lines to the data, using slope as the only parameter. In the condition with S-cone disks and L&M-cone annuli (Fig. 4F), observer JL obtained an estimated null at the highest disk mean contrast that was far in excess of the estimates for the other two observers. The estimate of observer JL's null was 0.14. This estimate lies above the plot range in Fig. 4F and is excluded from fits. The normal, filled data points refer to the average results for the other two observers.

Lines fit the data well (see Table 2). The variance accounted for by the fit lines is at least 98% for all conditions and is greater than 99% for most of them. Again, the pattern of results agrees with results of our earlier experiment on chromatic selectivity.[3] Contrast induction is strongest when disk and annulus share the same cardinal axis (Figs. 4A, 4E, and 4I), and annulus contrast modulation at isoluminance has but a small effect on the appearance of achromatic contrast (Figs. 4D and 4G). We are at a loss to explain the small dips that are evident at the third disk mean contrast level in each panel. These dips are evident in the data of individual observers JL and BS but not JC.

The linear fits show that induced modulation of contrast in a central disk depends approximately linearly on disk mean contrast, at low to moderate contrast levels, in the three dimensions of color space. This result is the

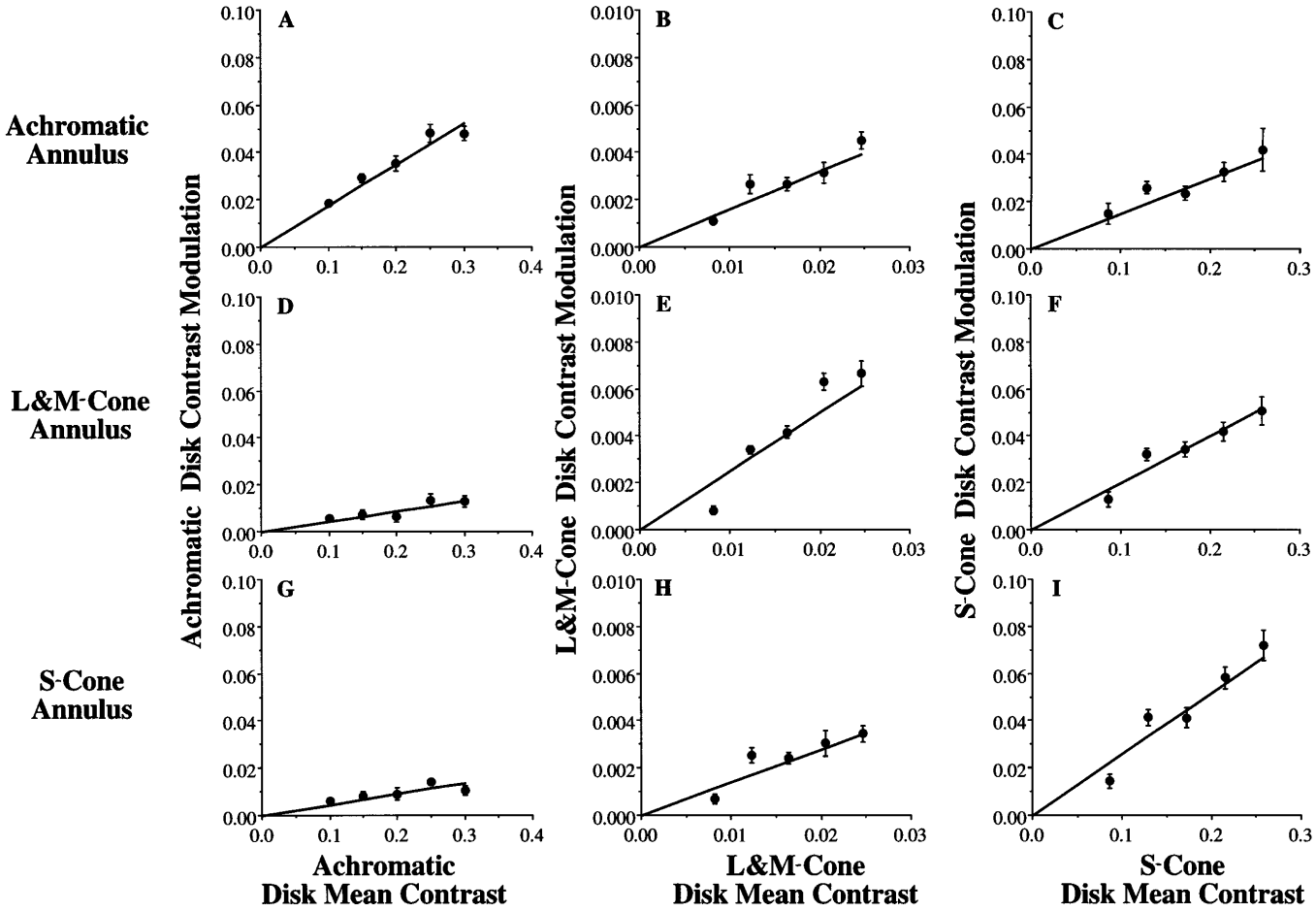

Fig. 4. Dependence of contrast induction on disk mean contrast. The format is like that of Fig. 3; results are for the three observers JC, JL, and BS. Panels in the left, middle, and right columns describe results with disks along the achromatic, L&M-cone, and S-cone axes, respectively. Panels in the top, middle, and bottom rows describe results with annuli along the achromatic, L&M-cone, and S-cone axes, respectively. See text for details.

Table 2. Slopes of Lines Fitted to the Data in Fig. 4 and Goodness of Fit

Condition (Disk, Annulus)	Slope	R^2
A, A	0.176	0.993
L&M, A	0.159	0.999
S, A	0.153	0.993
A, L&M	0.046	0.997
L&M, L&M	0.252	0.998
S, L&M	0.194	0.993
A, S	0.046	0.995
L&M, S	0.137	0.999
S, S	0.259	0.988

second support of a bilinear model for the chromatic properties of contrast gain control.

4. BILINEAR MODEL FOR THE EFFECTS OF CONTRAST MODULATION

The model is designed to predict the physical change in the lights from a central area that is needed to make its color appearance constant across changes in lights from surrounding areas. We develop the model in stages; here we focus on predicting the results of the experiments presented above. The specific aim is to predict the modulation of a central disk that nulls the apparent modulation induced by modulating annulus contrast. Later in the paper we develop the model more generally.

A. Formalism

We consider three variables. The first two are independent variables in the experiments and include the disk mean contrast vector $\mathbf{d}$ and the annulus contrast modulation vector $\boldsymbol{\alpha}$ [Eqs. (1) and (2)]. The third is a dependent variable, namely, the disk contrast modulation $\boldsymbol{\nu}$ that nulls the induced modulation. We represent each of these variables by a three-dimensional (column) vector in color space: $\mathbf{d} = [d_1\ d_2\ d_3]^T$, $\boldsymbol{\alpha} = [\alpha_1\ \alpha_2\ \alpha_3]^T$, and $\boldsymbol{\nu} = [\nu_1\ \nu_2\ \nu_3]^T$, where the superscript ^{T} denotes transpose. The indices refer to particular axes in color space. We choose the first to refer to the achromatic axis, the second to the L&M-cone axis, and the third to the S-cone axis.

The aim is to use the disk mean contrast $\mathbf{d}$ and the annulus contrast modulation $\boldsymbol{\alpha}$ to predict the nulling modulation $\boldsymbol{\nu}$. The linear dependencies shown experimentally suggest a bilinear model that maps the two vectors $\mathbf{d}$ and $\boldsymbol{\alpha}$ into the third vector $\boldsymbol{\nu}$. The defining properties of a bilinear model are two. To express these properties, call the bilinear mapping B and

suppose that c_1, c_2, e_1, and e_2 are scalar multipliers; $\mathbf{d}_1$, $\mathbf{d}_2$, and $\mathbf{d}$ are mean disk contrasts; and $\boldsymbol{\alpha}_1$, $\boldsymbol{\alpha}_2$, and $\boldsymbol{\alpha}$ are modulations of annulus contrast. A bilinear model represented by the mapping B must then satisfy[31] both

$$B(c_1\mathbf{d}_1 + c_2\mathbf{d}_2, \boldsymbol{\alpha}) = c_1B(\mathbf{d}_1, \boldsymbol{\alpha}) + c_2B(\mathbf{d}_2, \boldsymbol{\alpha})$$

and

$$B(\mathbf{d}, e_1\boldsymbol{\alpha}_1 + e_2\boldsymbol{\alpha}_2) = e_1B(\mathbf{d}, \boldsymbol{\alpha}_1) + e_2B(\mathbf{d}, \boldsymbol{\alpha}_2)\,; \qquad (3b)$$

that is, the bilinear mapping B must be linear in the first variable (disk mean contrast) and in the second variable (annulus contrast modulation).

The general form of such a bilinear model can be expressed with use of bilinear model matrices $\mathbf{B}_1$, $\mathbf{B}_2$, and $\mathbf{B}_3$ as follows[21–25]:

$$\nu_k = \sum_{j=1}^{3}\sum_{i=1}^{3} d_j(\mathbf{B}_j)_{ki}\alpha_i \qquad \text{for } k = 1, 2, 3\,, \qquad (4a)$$

or written out fully:

$$\begin{bmatrix}\nu_1\\ \nu_2\\ \nu_3\end{bmatrix} = \left\{ d_1\begin{bmatrix} b_{111} & b_{112} & b_{113}\\ b_{121} & b_{122} & b_{123}\\ b_{131} & b_{132} & b_{133}\end{bmatrix} + d_2\begin{bmatrix} b_{211} & b_{212} & b_{213}\\ b_{221} & b_{222} & b_{223}\\ b_{231} & b_{232} & b_{233}\end{bmatrix} + d_3\begin{bmatrix} b_{311} & b_{312} & b_{313}\\ b_{321} & b_{322} & b_{323}\\ b_{331} & b_{332} & b_{333}\end{bmatrix}\right\}\begin{bmatrix}\alpha_1\\ \alpha_2\\ \alpha_3\end{bmatrix}. \qquad (4b)$$

Each of the bilinear model matrices $\mathbf{B}_1$, $\mathbf{B}_2$, and $\mathbf{B}_3$ is 3×3 in size. The matrix with index j has indices b_{jki} or $(\mathbf{B}_j)_{ki}$, as in Eq. (4a). Each matrix has 9 entries, for a total of 27 numbers needed to specify the model.

A considerable simplification can be made: only three entries per matrix need be determined, because most of the model matrix entries are zero:

$$\begin{bmatrix}\nu_1\\ \nu_2\\ \nu_3\end{bmatrix} = \left\{ d_1\begin{bmatrix} b_{111} & b_{112} & b_{113}\\ 0 & 0 & 0\\ 0 & 0 & 0\end{bmatrix} + d_2\begin{bmatrix} 0 & 0 & 0\\ b_{221} & b_{222} & b_{223}\\ 0 & 0 & 0\end{bmatrix} + d_3\begin{bmatrix} 0 & 0 & 0\\ 0 & 0 & 0\\ b_{331} & b_{332} & b_{333}\end{bmatrix}\right\}\begin{bmatrix}\alpha_1\\ \alpha_2\\ \alpha_3\end{bmatrix}. \qquad (5)$$

The reason for this simplification is an empirical result stated above. When disk chromatic properties are restricted to lie along one of the three cardinal axes, induced modulation takes the form of a modulation of apparent contrast along the disk axis. To see how this restricts the bilinear model matrices, consider the change in appearance of an achromatic disk, with some contrast $[d_1\ 0\ 0]^T$, caused by annulus modulation. The nulling modulation is achromatic and so has the form $[\nu_1\ 0\ 0]^T$, no matter what the axis of the annulus contrast modulation is. Equation (4b) shows immediately that the two lowermost rows of $\mathbf{B}_1$ must be zero. Similar arguments concerning disks along the second and third color-space axes zero the corresponding entries in $\mathbf{B}_2$ and $\mathbf{B}_3$. We show below in Subsection 5.C that this restriction on the form of the bilinear model corresponds to plausible and simple circuitry for the contrast gain control.

B. Numerical Specification

To determine a working bilinear model we must specify the nine nonzero entries of the bilinear model matrices [Eq. (5)]. Each entry describes a linear increase in nulling contrast with increasing annulus contrast modulation, for some choice of disk color axis and annulus color axis. The nine nonzero entries evidently correspond to the slopes of the best-fit lines (with intercept zero) found in the experiment on the effects of annulus contrast modulation (see Fig. 3). These slopes are presented in the second column of Table 1. The slopes across the top row of Fig. 3 (results for achromatic disks in Figs. 3A, 3B, and 3C) correspond, from left to right, to entries b_{111}, b_{112}, and b_{113} of matrix $\mathbf{B}_1$; the slopes across the middle row (results for L&M-cone-axis disks, Figs. 3D, 3E, and 3F) correspond to entries b_{221}, b_{222}, and b_{223} for matrix $\mathbf{B}_2$; and the slopes across the bottom row (results for S-cone-axis disks, Figs. 3G, 3H, and 3I) correspond to entries b_{331}, b_{332}, and b_{333} for matrix $\mathbf{B}_3$.

The bilinear model matrix entries are expressed in terms of standard contrast units along the achromatic axis, in terms of contrast to L cones along the L&M-cone axis, and in terms of contrast to S cones along the S-cone axis. Because the slopes in Fig. 3 were determined experimentally with disks at 30% of the maximum displayable contrast, the slopes must be corrected to provide the actual bilinear model matrix entries. One must multiply each slope by the reciprocal of 30% of the maximum displayable contrast to the appropriate cone mechanism to determine the corresponding model entry. For the slopes found with achromatic disks, the appropriate multiplicative factor is $3.33 = 1/(30\% \times 100\%)$; for L&M-cone-axis disks, the factor is $40.65 = 1/(30\% \times 8.2\%)$; and for S-cone-axis disks the factor is $3.88 = 1/(30\% \times 86\%)$. The bilinear model matrix entries that result from the data of Fig. 3 are presented in the second column of Table 3.

C. Transposed Model

The data in Fig. 4, which concern the effects of changing disk mean contrast, can also be used to specify a bilin-

Table 3. Bilinear Model Parameters[a]

Parameter ($b_{ji} = b_{jji}$)	Fig. 3	Fig. 4	Fig. 5		Fig. 7
			Sinusoid	Noise	
b_{11}	0.765	0.878	0.64	0.67	0.695
b_{21}	0.483	0.797	0.78	0.54	0.952
b_{31}	0.796	0.766	0.86	0.77	0.924
b_{12}	2.18	2.78	0.51	0.89	1.41
b_{22}	14.7	15.4	15.0	14.87	14.38
b_{32}	13.3	11.9	14.4	11.7	14.10
b_{13}	0.148	0.265	0.04	0.08	0.10
b_{23}	0.686	0.795	1.36	0.43	0.917
b_{33}	1.41	1.51	1.48	1.54	1.63

[a]The estimates are derived as follows: in the second column, from the average data of three observers in an experiment in which annulus contrast modulation was varied (Fig. 3); in the third column, from the average data of three observers in an experiment in which disk mean contrast was varied (Fig. 4); in the fourth column, from the average data of four observers in an experiment in which horizontally oriented sinusoidal stimuli were used (Fig. 5, filled bars); in the fifth column, from the average data of four observers in a parallel experiment in which binary noise was used (Fig. 5, open bars); in the sixth column, from the average data of three observers in an experiment in which annulus mean contrast was varied (Fig. 7).

ear model. This model transposes the roles of annulus contrast modulation and disk mean contrast. In terms of the transposed bilinear model matrices $\mathbf{B}_1'$, $\mathbf{B}_2'$, and $\mathbf{B}_3'$, we have

$$\nu_k = \sum_{i=1}^{3}\sum_{j=1}^{3} \alpha_i (\mathbf{B}_i')_{kj} d_j \qquad \text{for } k = 1, 2, 3. \tag{6a}$$

The entries $b_{ikj}' = (\mathbf{B}_i')_{kj}$ of the transposed matrices are related to the entries $b_{jki} = (\mathbf{B}_j)_{ki}$ of the original matrices in the following way: $b_{ikj}' = b_{jki}$. In terms of entries b_{jki} of the original bilinear model matrices $\mathbf{B}_1$, $\mathbf{B}_2$, and $\mathbf{B}_3$ of Eq. (5), the transposed model is expressed more fully as

$$\begin{bmatrix}\nu_1\\ \nu_2\\ \nu_3\end{bmatrix} = \left\{ \alpha_1 \begin{bmatrix} b_{111} & 0 & 0\\ 0 & b_{221} & 0\\ 0 & 0 & b_{331}\end{bmatrix} + \alpha_2 \begin{bmatrix} b_{112} & 0 & 0\\ 0 & b_{222} & 0\\ 0 & 0 & b_{332}\end{bmatrix} + \alpha_3 \begin{bmatrix} b_{113} & 0 & 0\\ 0 & b_{223} & 0\\ 0 & 0 & b_{333}\end{bmatrix} \right\} \begin{bmatrix} d_1\\ d_2\\ d_3\end{bmatrix}, \tag{6b}$$

and it is evident that the transposed bilinear model matrices are diagonal.

The slopes in the plots across the top row of Fig. 4 (results for achromatic modulations of annulus contrast, Figs. 4A, 4B, and 4C) correspond, from left to right, to entries b_{111}, b_{221}, and b_{331}; the slopes across the middle row (results for L&M-cone-axis annuli, Figs. 4D, 4E, and 4F) correspond to entries b_{112}, b_{222}, and b_{332}, and the slopes across the bottom row (results for S-cone-axis annuli, Figs. 4G, 4H, and 4I) correspond to entries b_{113}, b_{223}, and b_{333}.

Again, if the slopes are to provide bilinear model matrix entries, then they must be corrected to account for the fixed annulus modulation level of 20% of the maximum displayable contrast used in the experiments. The slopes must be multiplied by the reciprocal of 20% of the maximum displayable contrast to the appropriate cone mechanism. For achromatic annuli the slopes must be multiplied by $5.0 = 1/(20\% \times 100\%)$; for L&M-cone annuli the factor is $60.98 = 1/(20\% \times 8.2\%)$; and for S-cone annuli the factor is $5.81 = 1/(20\% \times 86\%)$. The resulting estimates of the bilinear model matrix entries, found from the data presented in Fig. 4, are presented in the third column of Table 3.

Each of the values in the second and third columns of Table 3 specifies the bilinear model for the average of three observers. The estimates of the bilinear model matrix entries that arise from the experiment that varied annulus contrast modulation (second column) are very similar to those that arise from the experiment that varied disk mean contrast (third column). In only two cases is there a discrepancy. The first involves the effects of achromatic modulation on L&M-cone disk appearance (b_{221}); the estimate 0.483 provided by the annulus modulation data in Fig. 3 is only ~60% of the estimate 0.797 provided by the disk contrast data in Fig. 4. This is also true of the estimates 0.148 and 0.265 for the effects of S-cone-axis modulation on achromatic appearance (b_{113}). We have no reason to believe that these discrepancies are due to anything other than unsystematic error. As discussed below in Subsection 4.E, these discrepancies do not produce substantial changes in model predictions.

Note that one can estimate the nine numbers needed to specify the bilinear model most simply by finding a single nulling modulation for each of the nine disk and annulus color-axis combinations. Given bilinearity at low and moderate contrasts, only nine data points must be determined experimentally for estimation of an observer's bilinear model.

We may also simplify notation. Two indices rather than three are needed for each bilinear model parameter, because only those parameters b_{jki} for which $j = k$ are nonzero. We thus rewrite the nonzero parameter b_{jji} as b_{ji} for $i, j = 1, 2, 3$ in what follows.

D. Spatially Sinusoidal Stimuli

We tested how well results with binary noise stimuli match results found with spatially sinusoidal stimuli. Although our primary aim with the sinusoidal stimuli is to control for possible luminance artifacts, the experimental results also provide an opportunity for us to illustrate the estimation of bilinear model matrix entries using only nine measurements per observer.

As described in our earlier paper,[3] the use of horizontally oriented sinusoids minimizes several types of luminance artifact associated with the display of binary noise patterns that are nominally isoluminant. The artifacts include raster display artifacts, associated especially with vertical edges, and both longitudinal and lateral chromatic aberration. The spatial properties of the sinusoidal stimuli are depicted in the inset in Fig. 5. The spatial frequency was set to 2 cycles/deg, which is close to the peak frequency of the binary noise pattern (1.8 cycle/deg).

Observers viewed sinusoidal stimuli in nine experimental conditions that correspond to the nine possible color-axis combinations. In parallel, the observers participated in a second set of nine conditions in which they viewed isotropic binary spatial noise, as in the experiments described above. Nulling modulations were determined with the method of limits, as described in our earlier work.[3]

Results are shown in Fig. 5. Nulls determined with the spatial sinusoids are indicated by filled bars; nulls found with the binary noise are indicated by open bars. The displayed nulls are the averages of nulls collected by the four observers, BS, JH, JL, and LD. Disk and annulus mean contrasts were fixed at 30% of the maximum displayable contrasts along their respective axes. The amplitude of annulus contrast modulation was fixed at 20% of the maximum. As in the experiments described above, the vertical axes are scaled in terms of contrast to appropriate cone mechanisms.

The results show that contrast induction is comparable for the sinusoidal and the binary noise stimuli for all conditions except one (S-cone annulus, L&M-cone disk), in which induction is significantly greater with the sinusoidal stimuli than with the binary noise patterns. We have no explanation for this anomaly. The strong similarity of the results suggests that the results with isoluminant binary noise stimuli reflect chromatic processing rather than the sequelae of luminance artifacts. The results also display the chromatic selectivity and the neg-

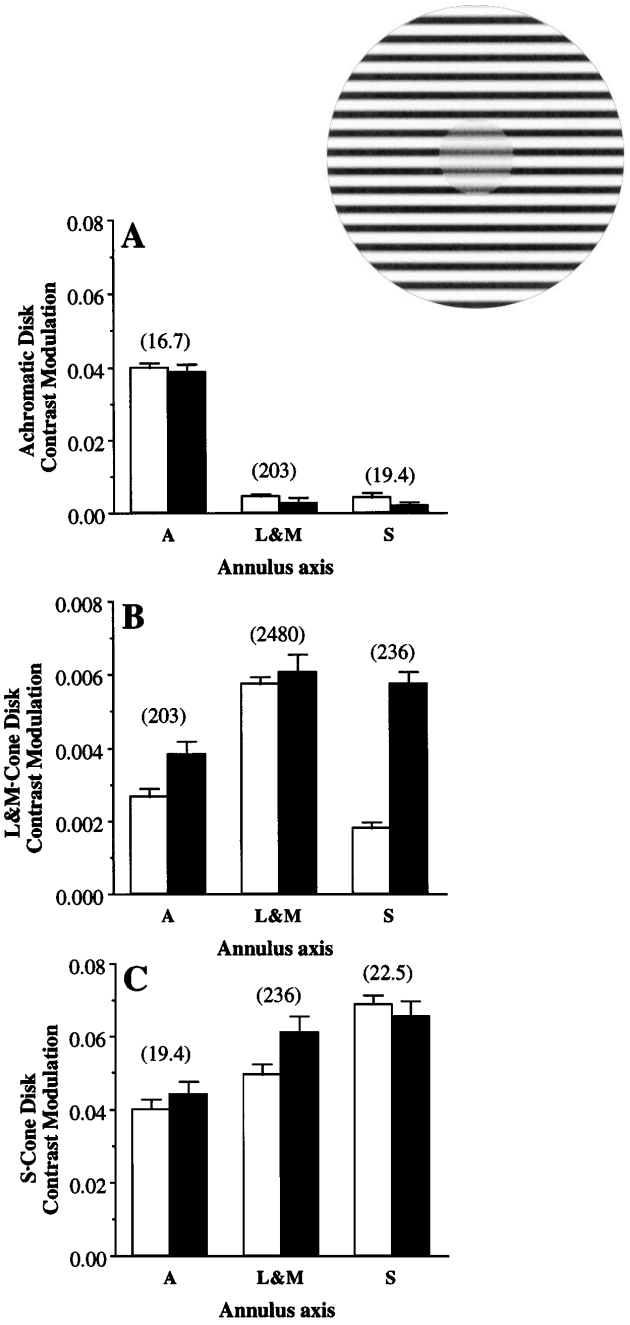

Fig. 5. Results with horizontally oriented sinusoids at 2 cycles/deg (filled bars) and with binary spatial noise (open bars) for observers LD, JH, JL, and BS. A, B, and C show average nulling contrast modulations for achromatic, L&M-cone, and S-cone disks, respectively. The color-space axis of the annulus varies across the bottom of each panel. The numbers in parentheses at the tops of the columns are the scale factors that are needed to turn these nulling modulations, expressed in terms of contrast to appropriate cone mechanisms, into the bilinear model matrix entries of Table 3 (fourth and fifth columns). See text for details.

ligible effect of isoluminant contrast modulation on apparent achromatic contrast that were described above and in earlier work,[3] although the chromatic selectivity suggested by the present results with sinusoids is rather weak.

Each set of nine measurements can be used to specify a bilinear model. The three measurements in Fig. 5A provide the three entries of bilinear model matrix $\mathbf{B}_1$, the measurements in Fig. 5B provide the entries of $\mathbf{B}_2$, and the measurements in Fig. 5C provide the entries of $\mathbf{B}_3$. As described earlier, one must scale each measurement appropriately to determine a bilinear model matrix entry that is scaled in terms of contrasts to the appropriate cone mechanisms. The proper factor is the reciprocal of the product of 30% of the maximum displayable contrast along the disk axis and 20% of the maximum displayable contrast along the annulus axis. These scale factors are provided in parentheses at the tops of the pairs of bars.

The bilinear model matrix entries that correspond to the results with horizontally oriented sinusoids are presented in the fourth column of Table 3. The fifth column displays the entries that correspond to the results with binary noise. The most significant discrepancies between the rapidly obtained estimates (Fig. 5) and the more painstaking estimates (Figs. 3 and 4) concern the effects of isoluminant contrast modulation on the appearance of achromatic contrast (entries b_{12} and b_{13}). These effects are small to start with, and rapid estimation has rendered them lower still.

E. Chromatic Selectivity of the Bilinear Model

We used the models specified by the experiments to predict the dependence of induced contrast on disk mean contrast and annulus contrast modulation, at low and moderate contrast levels.

Figure 6 shows bilinear model predictions from the data on the effects of annulus contrast modulation, which are averaged across three observers (Fig. 3 and Table 3, second column). The predictions are presented in the form of vector fields. Each of the nine panels shows the predicted nulling contrast modulations for disks in a particular plane in color space. In each panel the predicted nulls are calculated in response to an annulus contrast modulation along a particular color-space axis. The color-space axis of the annulus is marked either by inward pointing arrows along the circumference, in cases in which the annulus contrast modulation lies along an axis in the plane, or by the central rings, in cases in which the axis is perpendicular to the prediction plane. Each vector represents the size and the chromatic properties of the predicted null needed for a disk with contrast marked by the base of the arrow. These vector fields are symmetric on reflection through the origin.

Note that the nulls predicted for disks in planes spanned by pairs of cardinal axes must lie in the same plane as the disk. This is a consequence of Eq. (5). The model predicts that nulls have no contrast component along a particular cardinal axis unless the disk has a contrast component along that axis.

Figures 6A, 6B, and 6C show nulls for disks in the isoluminant plane in response to achromatic, L&M-cone-, and S-cone-axis annuli, respectively. Figures 6D, 6E, and 6F shows nulls for disks in the plane spanned by the achromatic and L&M-cone axes, again in response to achromatic, L&M-cone-, and S-cone-axis annuli, respectively. Finally, Figs. 6G, 6H, and 6I show predicted nulls for disks in the plane spanned by the achromatic and the S-cone axes.

Figure 6A shows the predicted nulls in the case of annulus contrast modulation along the achromatic axis and

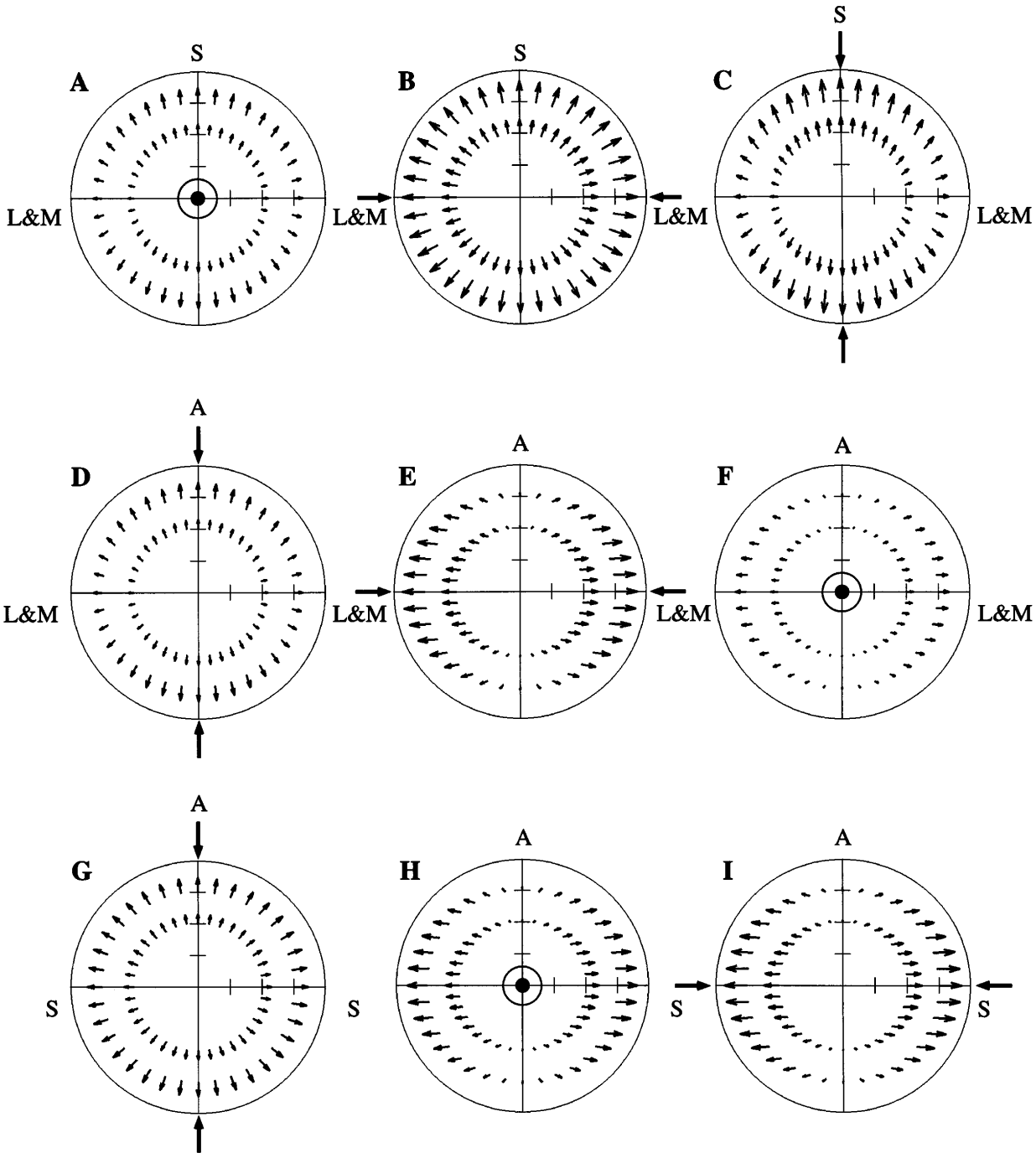

Fig. 6. Vector fields of nulling modulations that are predicted by the bilinear model of Eq. (5) specified in the second column of Table 3. Each circle represents a portion of a color plane spanned by two cardinal axes of color space, indicated at the top and at the side of each circle. The circle marks the 40% levels of maximum displayable contrast along each of the panel's cardinal axes; the tick marks represent 10% steps of maximum displayable contrast. The maximum displayable levels are 100% contrast along the achromatic axis, 8.2% contrast to L cones along the L&M-cone axis, and 86% contrast to S cones along the S-cone axis. Each vector shows the null predicted for the disk, with contrast marked by the base of the vector. The color-space axis of the annulus is indicated either by inward-pointing arrows at the circle circumference, in cases in which the cardinal axis of the annulus lies in the disk plane, or by circles at the center of the diagram, in cases in which the annulus axis is perpendicular to the disk color plane. Predictions are shown in A, B, and C for the effects of achromatic, L&M-cone-, and S-cone-axis modulations, respectively, on disks in the isoluminant plane; D, E, and F for the effects of achromatic, L&M-cone-, and S-cone-axis modulations, respectively, on disks in the plane spanned by achromatic and L&M-cone axes; and in G, H, and I for the effects of achromatic, L&M-cone-, and S-cone-axis modulations, respectively, on disks in the plane spanned by achromatic and S-cone axes. In generating these predictions, we set the annulus mean contrast to 30% and annulus contrast modulation to 20% of the corresponding maximum displayable contrasts. See text for details.

disks along axes in the isoluminant plane. In this and the other panels, the circular boundary passes through the points along the cardinal axes that correspond to 40% of the maximum displayable contrast. The corresponding cone contrasts are $40\% \times 8.2\% = 3.28\%$ contrast to L cones along the L&M-cone axis and $40\% \times 86\% = 34.4\%$ contrast to S cones along the S-cone axis. Predictions are displayed at disk mean contrast levels of 20% and

30% of the maximum displayable along the cardinal axes (forming two rings of vectors). These levels correspond to 1.64% and 2.46% to L cones and to 17.2% and 25.8% to S cones. Ticks mark 10% steps in contrast. For the predictions in this and the other panels the annulus mean contrast was set to 30% of the maximum displayable contrast and the annulus contrast modulation was set to 20%, which corresponds to a sinusoidal modulation of annulus contrast between 10% and 50%.

Figures 6A–6C show predictions for isoluminant disks of low to moderate contrast. In response to achromatic (Fig. 6A), L&M-cone- (Fig. 6B), and S-cone- (Fig. 6C) axis contrast modulation, isoluminant disks are predicted to undergo primarily a modulation of saturation: the nulling contrast modulation is largely along the disk axis. This is most clearly the case with L&M-cone-axis contrast modulation (Fig. 6B), which generates a nearly perfectly radial vector field. Induced modulation of apparent contrast deviates from radiality toward the S-cone axis in the cases of achromatic (Fig. 6A) and S-cone- (Fig. 6C) axis contrast modulation. The induced modulations in these cases involve small changes in disk hue in addition to the (radial) change in saturation.

Figures 6D–6F show predictions for disks with chromaticities in the plane spanned by the achromatic and the L&M-cone axes. The nulling modulations predicted in response to the modulation of achromatic contrast lie largely along the disk axis (Fig. 6D) and reflect the influence of achromatic contrast modulation on the appearance of both achromatic and isoluminant stimuli. On the other hand, the nulls in response to isoluminant contrast modulation (Figs. 6E and 6F) are themselves almost completely isoluminant. The vector fields in Figs. 6E and 6F reflect the largely negligible effect of contrast modulation at isoluminance on the appearance of achromatic contrast: little induced modulation is found for disks at and close to the achromatic axis, whereas induced modulation for disks with more substantial chromatic components is largely isoluminant.

Figures 6G–6I show predictions, finally, for disks with chromaticities in the plane spanned by the achromatic and the S-cone axes. Whereas the response to achromatic modulation is largely radial (Fig. 6G), the response to isoluminant modulation is largely isoluminant (Figs. 6H and 6I). These results (Figs. 6G–6I) are like those in Figs. 6D–6F.

The predictions displayed in Fig. 6 are derived from the data, averaged across observers, that were obtained in the experiment in which annulus contrast modulation was varied. We also generated vector-field predictions, using data from the experiment on disk mean contrast and using data from the experiment with horizontally oriented sinusoids. Visual comparison of the vector fields showed that each model's predictions are nearly identical. The only evident differences are found in the predictions for the effect of S-cone-axis modulation on isoluminant disks. The predictions of the results shown in Figs. 3 and 4 and in Fig. 5 for the binary noise stimuli resemble one another in departing from radiality: nulls in these cases tend toward the S-cone axis, as pictured in Fig. 6C. The predictions of the results for the sinusoidal stimuli, shown in Fig. 5, are more nearly radial in the case of S-cone-axis modulation on isoluminant disks. The difference between predictions for the binary noise stimuli and the sinusoidal stimuli is due to differences in the relative sizes of bilinear model matrix entries b_{23} and b_{33} (see Table 3).

5. TOWARD A MODEL FOR COLOR IMAGE PROCESSING

We now work to generalize the model. The first step is to extend the model to account for the effects of annulus contrast, rather than annulus contrast modulation, on central appearance. We test a fundamental prediction of the extended model in experiments on the effects of annulus mean contrast. The model predicts that nulls are independent of annulus mean contrast, and experimental results show that this prediction is met at low and moderate contrasts. The data collected at high contrasts, however, exhibit response saturation. We fitted the data by embellishing the bilinear model with saturating nonlinearities in the contrast gain control of each of the color channels. This is accomplished within the framework of a realization of the bilinear model as a feedforward, matrix-multiplicative contrast gain control.

A. Total Annulus Contrast

The bilinear model presented in Section 4 was created and specified to predict the results of experiments in which annulus contrast is modulated. Left ignored were the annulus mean contrast levels, which were fixed at 30% of the maximum displayable contrast along each of the color-space axes.

The model is extended most simply to treat variation in annulus mean contrast by the supposition that nulling modulation is related bilinearly to disk mean contrast and *total* annulus contrast, where total annulus contrast is the sum of mean and modulated contrast. The annulus mean contrast $\boldsymbol{\alpha}_m$ and the contrast modulation $\boldsymbol{\alpha}(t)$ [Eq. (2)] combine to give the total contrast $\mathbf{a}(t)$:

$$\mathbf{a}(t) = \mathbf{a}_m + \boldsymbol{\alpha}(t). \tag{7}$$

The extended bilinear model uses the total annulus contrast $\mathbf{a}(t)$ and the disk contrast $\mathbf{d}$ to predict the nulling modulation $\boldsymbol{\nu}$.

Let us call the extended bilinear model $\boldsymbol{B}$. When provided with values $\mathbf{d}$ and $\mathbf{a}(t)$ for disk and annulus, respectively, the model $\boldsymbol{B}$ returns the time-varying modulation $\boldsymbol{\nu}(t)$ that nulls the apparent change in disk contrast:

$$\boldsymbol{\nu}(t) = \boldsymbol{B}[\mathbf{d}, \mathbf{a}(t)] = \boldsymbol{B}[\mathbf{d}, \mathbf{a}_m + \boldsymbol{\alpha}(t)]. \tag{8}$$

Because the model $\boldsymbol{B}$ is bilinear, it is linear in its second (annulus) argument [Eq. (3b)], so that the nulling modulation is the sum of responses to annulus mean and to annulus modulation:

$$\boldsymbol{\nu}(t) = \boldsymbol{B}[\mathbf{d}, \mathbf{a}_m] + \boldsymbol{B}[\mathbf{d}, \boldsymbol{\alpha}(t)]. \tag{9}$$

This equation makes a clear prediction concerning the effects of varying the annulus mean contrast on the time-varying nulling modulation. Because the bilinear model response to the annulus mean contrast does not vary in time, the time-dependent null that we measure experimentally, which is a zero-mean modulation of contrast,

should not vary with annulus mean contrast. The annulus mean contrast produces a steady reduction in the apparent contrast of the disk that is not captured with the nulling technique.

A second implication of Eq. (9) is that the earlier bilinear model, which we developed using data collected with annuli at mean contrasts of 30%, should continue to describe the extended model's predictions concerning annuli at other mean contrasts. When stripped of its mean, the time-varying nulling modulation predicted by the model is given by the old bilinear model response to the annulus contrast modulation and the disk mean contrast:

$$\boldsymbol{\nu}(t) - \boldsymbol{B}[\mathbf{d}, \mathbf{a}_m] = \boldsymbol{B}[\mathbf{d}, \boldsymbol{\alpha}(t)]. \tag{10}$$

Thus the estimates of bilinear model parameters that we gathered at annulus mean contrasts of 30%, using nulling modulations of mean zero, continue to specify the more general bilinear model.

B. Experimental Results on the Effects of Annulus Mean Contrast

We measured nulling contrast modulations in experiments in which annulus mean contrast was varied. Results were compared with the constant levels of nulling modulation predicted by the model.

Each experimental condition corresponded to a particular choice of one of the nine possible combinations of cardinal axes for disk and annulus. The color-space axis for the annulus mean contrast was held identical to the axis for the annulus contrast modulation. The disk was always presented with a mean contrast fixed at 30% of the maximum displayable contrast along its color-space axis. The annulus contrast modulation was also held fixed at an amplitude of 20% of the maximum displayable contrast along its axis in color space.

On a given trial, annulus mean contrast was chosen randomly from the range 20–60%, represented at 10% steps, of the maximum displayable contrast. Note that an annulus mean contrast of 20% is the lowest possible, given the choice to present an annulus contrast modulation of 20%. The annulus mean contrast and the contrast modulation always shared the same axis in color space. The disk contrast modulation presented on a particular trial was drawn from a range of values that spanned the nulling modulation and shared the color-space axis of the disk.

The results are shown in Fig. 7. The data are averaged across three observers. The color-space axis for both the mean and the modulation of the annulus varies from left to right. Results in the left, central, and right columns are for achromatic-, L&M-cone- and S-cone-axis annuli, respectively. The color-space axis of the disk varies from top to bottom. Results in the top, middle, and bottom rows are for achromatic, L&M-cone-, and S-cone-axis disks, respectively.

The annulus mean contrast varies along the horizontal axis in each of the plots, in units specific to the cardinal axis of the annulus. The amplitude of disk modulation that is needed to null the apparent change in disk contrast varies along the vertical axis in each of the plots, in units specific to the disk axis.

The data points show the nulling modulations averaged across three observers; error bars show estimates of the standard error of the mean. At the 20% annulus contrast level in Figs. 7D and 7G, one of the observers (JL) obtained nulls that were substantially in excess of those for the other two observers. Observer JL's data points are shown as open symbols in parentheses; these data are excluded from fits. The normal, filled symbols at 20% annulus mean contrasts in Figs. 7D and 7G refer to the average results from the other two observers.

The results show that the nulling modulation is approximately independent of annulus mean contrast, as predicted by the model, in four of the conditions. These four conditions include the three conditions with an achromatic disk (Figs. 7A–7C) and the condition with an S-cone annulus and an L&M-cone disk (Fig. 7F).

In the other conditions (Figs. 7D–7I) the results show that the nulling modulation is independent of annulus mean contrast for low and moderate contrasts and that the nulls are reduced at high annulus mean contrasts. These data suggest that there may be saturating nonlinearities in the action of the contrast gain control.

The annulus contrast values at which saturation is first evident in the data of Fig. 7 correspond roughly to estimates of those values provided by earlier data. For achromatic signals, data in Fig. 7A suggest that saturation starts at achromatic contrasts in the range 70–80%. Recall that the horizontal axis marks annulus mean contrast and that a further 20% modulation is added to the mean. The saturation evident in Fig. 7A at 50–60% annulus mean contrast thus corresponds to saturation at contrasts of 70–80%. This value agrees well with the estimate 70–80% provided by the data in the earlier paper (Fig. 4 of Ref. 3) but is somewhat higher than the estimate of 60% provided by the data in Fig. 3A of the current paper. For L&M-cone-axis signals, data in Fig. 7E show saturation onset at ~50–60% of the maximum displayable contrast of 8.2% to L cones. This value is lower than the 70–80% estimate provided by the data in the earlier paper (Fig. 4 of Ref. 3). Data in Fig. 3E suggest that the onset of saturation lies at or above 60%. Finally, for S-cone-axis signals, data in Fig. 7I show that the onset of saturation occurs at ~50–60% of the maximum displayable contrast of 86% to S cones. This is somewhat lower than the 70–80% estimate provided by data in the earlier paper[3] but agrees well with the estimate provided by the data in Fig. 3I.

The dashed lines mark the constant levels of induction that are predicted by the bilinear model, with use of the bilinear model matrix entries provided by the experiment on annulus contrast modulation (Fig. 3 and Table 3, second column). The predictions are those for disks of mean contrast of 30% and annulus contrast modulations of 20% of the maximum displayable levels along the appropriate axes in color space. With the exception of the data in Fig. 7D (achromatic annuli, L&M-cone disks), the predictions of the bilinear model provide a first-order fit that may be improved if we further suppose than the contrast gain control includes saturating nonlinearities.

The curve in each panel of Fig. 7 shows the fit provided by a model that includes saturating nonlinearities; these are detailed below. We turn first to a realization of

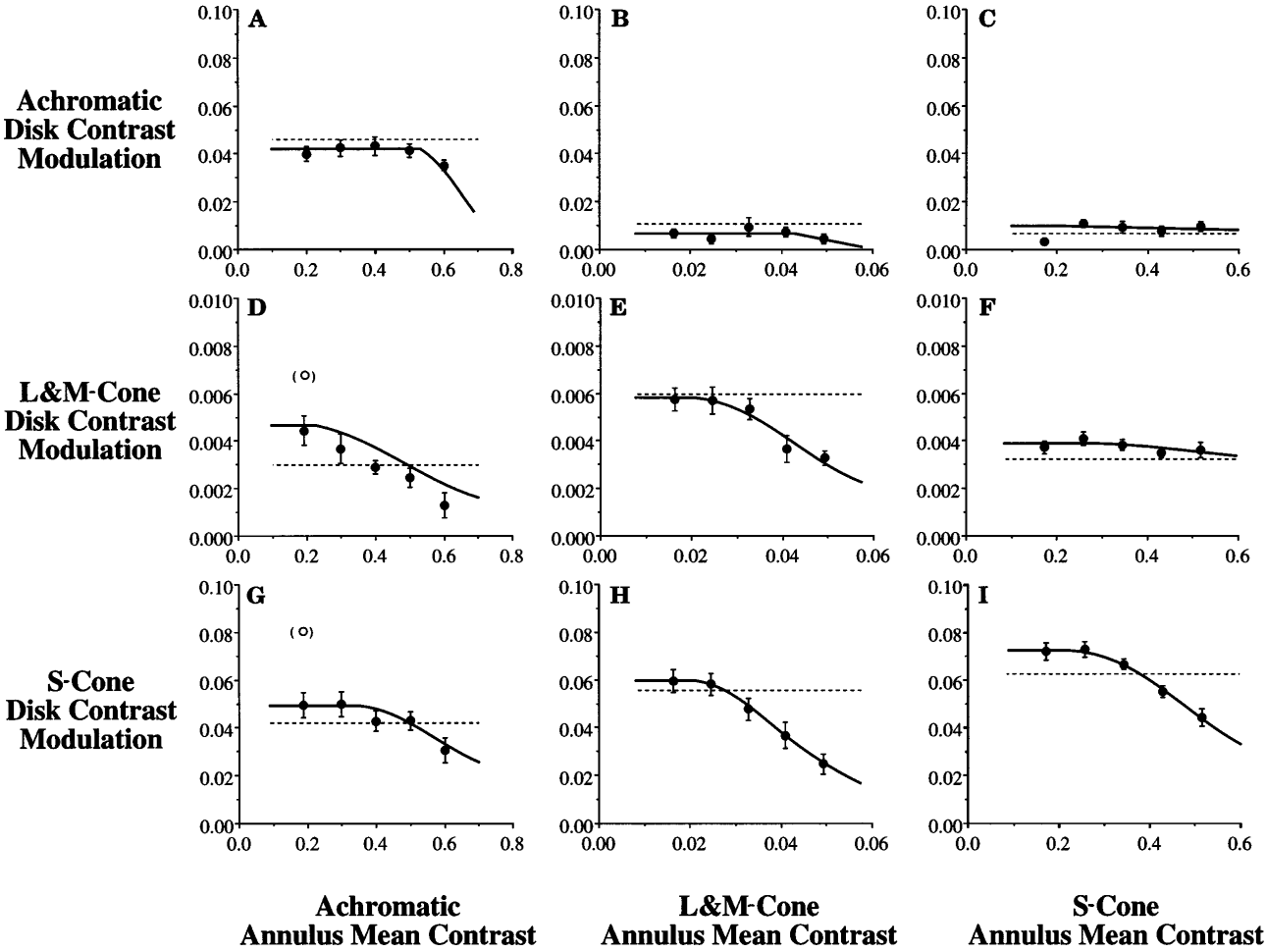

Fig. 7. Dependence of contrast induction on annulus mean contrast. The format is like that of Fig. 3; results are for the three observers JC, JL, and BS. At the lowest annulus mean contrasts, using achromatic annuli and isoluminant disks (D and G), observer JL obtained nulls far in excess of those for the other two observers. In these conditions observer JL's data are shown as open symbols in parentheses and are excluded from the fits, whereas the normal, filled data points at 20% annulus mean contrast levels refer to the average results for the other two observers. The dashed lines are the predictions of the bilinear model with parameters taken from the experiment on the effects of annulus contrast modulation (Fig. 3 and Table 3, column 2). The solid curves are the fits to the data of a bilinear model with saturating nonlinearities. See text for details.

the bilinear model as a feed-forward multiplicative gain control. We use this realization to help understand and quantify the saturating nonlinearities.

C. Feed-Forward Matrix-Multiplicative Contrast Gain Control

To implement the bilinear model using feed-forward multiplicative circuitry, we use the transposed version of the model [Eq. (6b)] and provide it a total annulus contrast argument $\mathbf{a} = [a_1\ a_2\ a_3]^T$:

$$\boldsymbol{\nu} = (a_1\mathbf{B}_1' + a_2\mathbf{B}_2' + a_3\mathbf{B}_3')\mathbf{d}\,. \tag{11}$$

The null $\boldsymbol{\nu}$ represents the way in which central contrast is reduced by surrounding contrast but bears a sign that is opposite to that of the induced contrast. The reduced disk contrast $\mathbf{d}'$ that results from the action of the contrast gain control is thus given by

$$\mathbf{d}' = \mathbf{d} - \boldsymbol{\nu} \tag{12a}$$

or

$$\mathbf{d}' = (\mathbf{I} - \mathbf{M})\mathbf{d}\,, \tag{12b}$$

in which $\mathbf{I}$ is the 3×3 identity matrix and $\mathbf{M}$ is the 3×3 diagonal matrix with elements

$$\begin{aligned} m_{11} &= a_1b_{11} + a_2b_{12} + a_3b_{13}\,, \\ m_{22} &= a_1b_{21} + a_2b_{22} + a_3b_{23}\,, \\ m_{33} &= a_1b_{31} + a_2b_{32} + a_3b_{33}\,. \end{aligned} \tag{13}$$

To simplify notation, set $m_1 = m_{11}$, $m_2 = m_{22}$, and $m_3 = m_{33}$. When written out fully, Eq. (12b) then reads as

$$\begin{bmatrix} d_1' \\ d_2' \\ d_3' \end{bmatrix} = \begin{bmatrix} 1 - m_1 & 0 & 0 \\ 0 & 1 - m_2 & 0 \\ 0 & 0 & 1 - m_3 \end{bmatrix} \begin{bmatrix} d_1 \\ d_2 \\ d_3 \end{bmatrix}. \tag{14}$$

Figure 8 shows the feed-foward multiplicative gain control that corresponds to Eqs. (13) and (14). This gain control acts at the second stage of color processing. The first stage is represented at the very top of the diagram by the L-, M-, and S-cone photoreceptoral mechanisms and a simple form of gain control, namely, a von Kries–type normalization of cone mechanism responses.[32,33] We use the first stage of the model to normalize cone mechanism

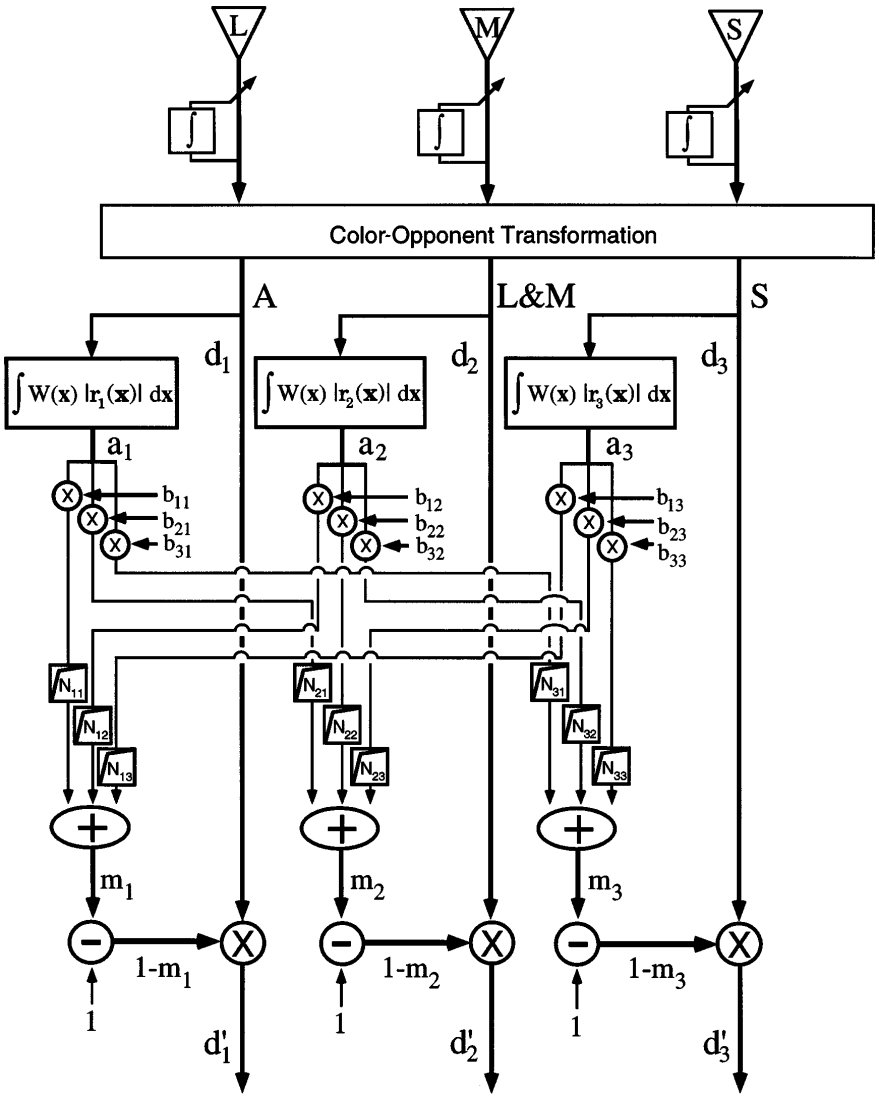

Fig. 8. Feed-forward matrix-multiplicative contrast gain control with saturating nonlinearities. An illustrative first stage (top) includes three cone mechanisms that undergo von Kries adaptation. A linear transformation characterizes the second-stage mechanisms in terms of responses along achromatic (A), L&M cone-, (L&M) and S-cone (S) axis dimensions. These responses $\mathbf{d} = [d_1\ d_2\ d_3]^T$ at a central position are multiplied by factors determined by the contrast gain control (bottom) to produce the normalized responses $\mathbf{d}'$. The local contrast in each channel's response $r_i(\mathbf{x})$ is pooled according to a pooling function $W(\mathbf{x})$. Contrast is determined by full-wave rectification of a second-stage mechanism's response. The local surround's contrast $\mathbf{a} = [a_1\ a_2\ a_3]^T$ is then multiplied by bilinear model matrix entries and fed to each of the color channels, where appropriate sums are taken to form the quantities $\mathbf{m} = [m_1\ m_2\ m_3]^T$ of Eq. (14). Saturating nonlinearities N act on the cross-channel connections before summation. We subtract the resulting sum for each channel from 1 to determine the channel's normalization factor $1 - m_j$ for $j = 1, 2, 3$. See text for details.

responses by the responses to the white point $\mathbf{w}$, which is the average light in the experiments.

We suppose that the visual input at each location in the visual field is represented by the responses $r_1(\mathbf{x})$, $r_2(\mathbf{x})$, and $r_3(\mathbf{x})$ of three second-stage mechanisms with sensitivities that correspond to achromatic, L&M-cone, and S-cone axes, respectively. The second-stage responses are determined by an appropriate linear transformation of cone mechanism responses. When the Smith–Pokorny[10] fundamentals are used, this linear transformation has a very simple form.[11] We strip the mean from the second-stage responses, so that the second-state response to the white point light is zero, viz., $[0\ 0\ 0]^T$.

The contrast gain control operates by multiplying the response $\mathbf{d} = [d_1\ d_2\ d_3]^T = \mathbf{r}(\mathbf{x}_0)$ at some particular location $\mathbf{x}_0$ by the diagonal matrix $\mathbf{I}-\mathbf{M}$ in componentwise fashion to produce the normalized response $\mathbf{d} = [d_1'\ d_2'\ d_3']^T$ of Eq. (14). The multiplication is shown at the bottom of Fig. 8. The normalizing terms arise through a chromatically selective combination of contrast in surrounding areas [Eqs. (13)]. Each of the color components a_1, a_2, and a_3 of the total contrast $\mathbf{a}$, in the area surrounding the location $\mathbf{x}_0$ with contrast $\mathbf{d}$, is determined by an integral. The integral sums across space the product of a spatial pooling function $W(\mathbf{x})$ and the full-wave rectified response $r_i(\mathbf{x})$ of the appropriate chromatic mechanism:

$$a_i = \int W(\mathbf{x})|r_i(\mathbf{x})|\mathrm{d}\mathbf{x} \qquad \text{for } i = 1, 2, 3\,. \tag{15}$$

We full-wave rectify the responses $r_i(\mathbf{x})$ of the second-stage mechanisms to determine contrast rather than square the responses (or rectify and then square them[27])

to preserve bilinearity. The form of the spatial pooling function is discussed below.

Figure 8 shows that the local contrast energies a_1, a_2, and a_3 of the three color channels are multiplied by the appropriate bilinear model matrix entries to provide signals that, when summed, determine the factors m_1, m_2, and m_3 [Eq. (14)] that govern the multiplicative gain control. In the absence of saturating nonlinearities, this feed-forward, matrix-multiplicative gain control is a bilinear contrast gain control that is chromatically selective.

D. Saturating Nonlinearities

We insert saturating nonlinearities in the contrast gain control of each color channel to help account for the data collected at high annulus contrasts (Fig. 7). To fit these data, we have supposed that the influence of contrast in one color channel on signals in a second (possibly identical) color channel is subject to saturation. As shown in Fig. 8, the resulting model has nine saturating nonlinearities.

The form of the nonlinearity that we use to fit the data is shown in Fig. 9 by the curve labeled Medium. The curve belongs to a two-parameter family of curves that saturate in a way that is intermediate to the soft saturation of the exponential $1 - \exp(-t)$ (Fig. 9, Soft) and the hard nonlinearity described by the line segments (Fig. 9, Hard). Each of the curves that we use has a first parameter for the degree of saturation and a second parameter for the asymptote.

Appendix A describes in detail the action of the saturating nonlinearities and their effect on predicted nulling contrast modulations.

The full model provides each color channel interaction with a nonlinearity, for a total of 18 parameters: 9 nonlinearities times 2 parameters per nonlinearity. We found that we were able to fit the data of Fig. 7 adequately if we let all 18 parameters vary freely, in addition to varying the 9 bilinear model parameters b_{ji}, $i, j = 1, 2, 3$. The fits of the model with saturating nonlinearities to the data in Fig. 7 are shown by the solid curve in each panel of that figure. With the exception of the fit in Fig. 7D (achromatic annulus, L&M-cone disk), the fits are excellent. Yet the large number of parameters makes for a somewhat unsatisfactory state of affairs: 27 parameters fit 45 data points.

The estimates of the bilinear model parameters that result from fitting the model with saturating nonlinearities to the data in Fig. 7 are listed in the rightmost column of Table 3. These estimates are very similar to those provided by the earlier experiments. The estimates of the two parameters for each of the nine saturating nonlinearities are listed in Table 4. To each of the nine combinations of cardinal axes corresponds a saturating nonlinearity. The column labeled c lists the estimates of the parameter that sets the degree of saturation (from medium at 0 to hard at 1) for each of the nine nonlinearities. The column labeled r_{max} lists the estimates of the parameter that corresponds to asymptotic value.

Cases in which r_{max} exceeds unity are potentially a problem, because a sum m [Eqs. (13) and (14)] that exceeds 1 will provide, when subtracted from 1, a multiplicative scalar that is negative, thus reversing signal contrast (see Fig. 8). Although the asymptotic values were allowed to vary freely in the fit, there are only two cases in which estimates of r_{max} exceed 1. These describe the effects of S-cone contrast on isoluminant signals. The value is only 1.1 in these cases. In the case of S-cone disks and annuli, the model predicts that an S-cone annulus of contrast of 91% or greater to S cones will produce a contrast reversal of S-cone-axis signals. Although we believe that this is false, we have no way to test the prediction, because the maximum displayable contrast to S cones along the S-cone axis with our equipment is 86%. At 86% contrast no reversal is apparent. One can adjust the model to avoid the prediction of contrast reversal by changing the values 1.1 to values that are less than or equal to 1.0.

The disposition of the saturating nonlinearities described here is not the simplest possible. A simpler way that saturating nonlinearities might act in contrast gain control calls for three sites rather than nine. A single saturating nonlinearity in the gain control of each color channel can act at the level of the sum m, namely, after summation in each channel (see Fig. 8). We tried unsuccessfully to fit models of this sort to the data of Fig. 7.

6. DISCUSSION

We have presented a bilinear model for chromatic selectivity in contrast gain control. Several experiments tested and specified the model. First, the apparent modulation of disk contrast was shown to depend approximately linearly on the contrast modulation of an annular surround.

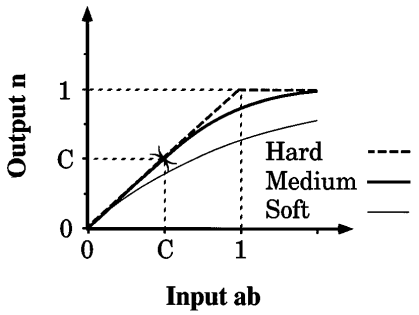

Fig. 9. Saturating nonlinearities. We use nonlinearities with an initial slope of 1 that are intermediate to the soft exponential $1 - \exp(-t)$ and the hard nonlinearity described by the line segments. The medium nonlinearities that we use splice together a straight-line segment for input values less than or equal to some constant c and a doubly exponential function with an initial slope of 1 for input values greater than c [Eqs. (A3)]. See text and Appendix A for details.

Table 4. Parameters c and r_{max} of the Saturating Nonlinearities Used to Fit the Data in Fig. 7

Condition (Disk, Annulus)	j, i	c	r_{max}
A, A	1, 1	0.511	0.540
L&M, A	2, 1	0.374	0.696
S, A	3, 1	0.481	0.788
A, L&M	1, 2	0.083	0.085
L&M, L&M	2, 2	0.521	0.895
S, L&M	3, 2	0.487	0.803
A, S	1, 3	0.063	0.357
L&M, S	2, 3	0.346	1.10
S, S	3, 3	0.633	1.10

Second, the apparent modulation was found to depend approximately linearly on the average contrast of the disk. These results were found for nine combinations of color-space axes for disk and annulus, at low and moderate contrasts. They are the basic supports of the bilinear model.

We confirmed our earlier finding that a disk with chromaticities along one of the cardinal axes changes in apparent contrast (achromatic axis) or apparent saturation (L&M-cone and S-cone axes) but not in hue.[3] This result allows the bilinear model to be specified by nine quantities that relate the three-dimensional chromatic description of the disk and the three-dimensional chromatic description of the annulus. These nine quantities were estimated in several ways, including a third experiment that used sinusoidal stimuli to control for luminance artifacts.

In a fourth experiment we examined the dependence of contrast induction on annulus contrast. We found that nulling modulation is independent of the average contrast of the annulus only at low-to-moderate contrast levels. To describe results at high contrast levels we include saturating nonlinearities in the contrast gain control of each chromatic channel. The nonlinearities are placed in a feed-forward, matrix-multiplicative model for contrast gain control.

A. Color

The initial impetus for using stimuli along the achromatic, L&M-cone, and S-cone axes came from the results of the chromatic habituation studies by Krauskopf and colleagues.[12,34] They showed that viewing slow flicker along the L&M-cone axis desensitizes the mechanisms that detect stimuli along this axis but has little effect on mechanisms that detect stimuli along the S-cone axis. Likewise, viewing slow flicker along the S-cone axis impairs S-cone-axis detectability and leaves L&M-cone detectability unscathed.

We found that a patterned disk along one of the cardinal axes in the isoluminant plane appears to change in color saturation but not in hue in response to modulating the contrast of a patterned annulus, while an achromatic disk appears to change in contrast. We call this property cardinal-axis invariance. As described in Subsection 4.B, cardinal-axis invariance leads to a considerable simplification in specifying a bilinear model. One reaps the benefits of this simplification if the basis axes that are used to express the model match the cardinal axes and one takes measurements for each of the nine cardinal-axis combinations to determine the nine matrix entries.

There is no strong reason to believe either that cardinal-axis invariance is precise or that it persists under substantial changes in experimental conditions. It is possible that cardinal-axis invariance holds only approximately under experimental conditions like those reported here. For instance, an approximate invariance may hold only for a small range of average lights and break down if the white point is colored. We have not tested this hypothesis.

Figure 6 shows that the induced modulations that are predicted for isoluminant disks lie largely along the chromatic axis of the disk. The modulations predicted for disks with an achromatic component that are induced by isoluminant modulation do not lie along the chromatic axis of the disk. Informal observations by us show that both of these predictions are qualitatively correct. One implication is that cardinal axes in the isoluminant plane need not be the true basis axes for contrast gain control. Although the cardinal axes of Krauskopf and colleagues[12,34] exhibit the invariance that leads to an important simplification in the model, other axes may possess the same property to a good approximation.

We encountered problems in our attempts to make observations of stimuli along intermediate axes. Our one-dimensional nulling procedure cannot be used to measure nulls that may vary in two dimensions, and, unfortunately, we were not successful in developing a reliable two-dimensional technique. The precision of candidate two-dimensional techniques was always far poorer than the precision of the one-dimensional technique used in the present experiments; this may be due, in part, to increased uncertainty.

That there need not be any cardinal axes whatever is suggested by models that include multiple mechanisms.[13,15,16,33,35] Models with multiple mechanisms include color-opponent mechanisms with peak responses to lights along axes that lie intermediate to cardinal axes. Electrophysiological evidence suggests that there are color-sensitive neurons in primate visual cortex that are tuned to intermediate color directions.[36]

The results of psychophysical habituation studies show that changes in detectability and appearance are always largest along the axis of habituation and smallest along the orthogonal axis. For instance, habituation to a slow modulation of chromaticity between the intermediate hues orange and blue-green produces the largest effects on the appearance and detectability of orange and blue-green tests and the smallest effects on yellow-green and violet tests. Yet a model that has mechanisms along cardinal axes always produces the greatest and the least effects along cardinal axes,[12,15,16,34] unless these cardinal-axis mechanisms change their spectral properties adaptively.[37,38]

It is possible to formulate a bilinear model for contrast gain control that has multiple mechanisms. Rather than possessing just three mechanisms at the second-stage level (as in Fig. 8), such a model possesses a large, finite number of mechanisms with different spectral peaks. The multiple-mechanism model relates nulling contrast bilinearly to disk and annulus contrast, encoded by all mechanisms, in a simple extension to the wiring diagram of Fig. 8. It is impossible to equate such a multiple-mechanism model with a simpler cardinal-axis model, despite the fact that the spectral sensitivities of intermediate mechanisms are related linearly to the sensitivities of cardinal-axis mechanisms. Rectifying the responses of mechanisms with intermediate sensitivities prevents the high-dimensional multiple-mechanism representation of contrast from being reduced to a low-dimensional cardinal-axis representation. Whether our results can be approximated well by a bilinear model with multiple mechanisms is an open question.

Contrast varies with changes in the opacity of visual media and is altered by fog, great distance, and the like. The contrast of a textured surface can also vary with changes in the spatial distribution of lighting and in the spatial orientation of the surface. The normaliza-

tion of opponent responses with respect to variations in contrast is thus helpful in visual recognition and in preserving channel bandwidth.[39] Contrast and saturation constancy[6] differ from color constancy, which concerns the effects of varying the chromatic properties of illumination. Changing the chromatic properties of illumination leads principally to shifts in the average light from a scene rather than to changes in scene contrast. That bilinear models have been used successfully to model the recovery of surface and light-source spectra from reflected lights[22–25] provides primarily a formal link between color constancy and the contrast constancies.

B. Space

Our model resembles the sketch of a spatially selective model for contrast gain control by Solomon and colleagues.[14] They suggest that the effects of contrast energy within particular spatial frequency channels on signals in other channels are mediated by cross-channel lines with variable intensive properties. The variable intensive properties for channel-specific inhibition discussed by Solomon and colleagues correspond to parameters in our model. Their distinction between early saturation and late saturation corresponds to our parameter $r_{\max}$. Their distinction between lower efficiency (same intercept) and higher efficiency (same intercept) corresponds to our parameter c. Finally, their distinction between lower efficiency (nonsaturating) and higher efficiency (nonsaturating) corresponds to our bilinear model parameters b_{ji}.

Solomon and colleagues follow the earlier models of Sperling[26] and Heeger[27] by suggesting that contrast measures are summed by the gain control of each channel and are then used in a divisive normalization procedure. Our measurements show that nulling contrast depends approximately linearly on annulus contrast modulation at low to moderate contrasts and saturates at higher contrasts. Although divisive normalization produces linear increase at low contrasts and saturation at higher contrasts, in agreement with our data, functions suggested in earlier work with divisive normalization[26,27] have a form that fits our data poorly.

Models of contrast gain control include some instantiation of the spatial pooling function that we term $W(\mathbf{x})$. This is a function of spatial position. It describes the linear summation of contrast energy within a local region that is presumably centered on the point at which the results of the contrast gain control are to be applied.

Two empirical studies[1,17] help to specify spatial pooling functions. Their results agree in showing that spatial pooling functions level off exponentially between annulus outer diameters of 4 and 6 deg of visual angle. This holds true for achromatic and isoluminant stimuli with peak energy in the spatial-frequency domain at ~2 cycles/deg. A problem with both of these studies is that the spatial pooling function within the central 2 deg of visual field is obscured by the measurement disk. This problem is manifest in the present study also. The bilinear model is specified with the use of data that pertain to disks of finite size, even though the contrast gain control is supposed to apply to signals at points in the visual field. In current work we pursue this problem and measure complete spatial pooling functions.[40]

Even a full specification of spatial pooling functions fails to provide a model of contrast gain control that can be applied to color images. The reason is that the contrast gain control is spatially as well as chromatically selective. Chubb and colleagues,[9] Cannon and Fullenkamp,[17] and Solomon and colleagues[14] showed that contrast gain control mechanisms are selective for stimulus spatial frequency and orientation. A consequence is that it is not sufficient simply to pool spatially the contrast in each of the three second-stage channels to determine gains for each channel. Rather, the contrast in each spatial frequency and orientation band must be pooled spatially in each of the three chromatic channels for gains to be determined for each spatiochromatic channel.

A bilinear model can be used to help describe spatiochromatic selectivity if apparent contrast induction can be shown to depend linearly on both center and surround contrasts across different spatial frequencies and orientations. In preliminary work we have found that bilinearity holds across different spatial frequencies and orientations, and we intend to pursue a bilinear model for contrast gain control that exhibits selectivity in the spatial frequency, orientation, and chromatic domains.

APPENDIX A: SATURATING NONLINEARITIES

A strictly bilinear model uses the factors m_1, m_2, and m_3 of Eq. (14) directly to set the gain: subtracting the factor m_j from 1 provides the multiplicative normalization factor for the jth chromatic channel for $j = 1, 2, 3$. Figure 8 shows that saturating nonlinearities act in each channel before the summation. We term these nonlinearities N_{ji}, where the index j refers to the chromatic channel at the place where gain is to be set (disk) and the index i refers to the chromatic channel in which surrounding contrast is measured (annulus). Each nonlinearity N_{ji} is a function that takes a single argument $a_i b_{ji}$ and produces a single output n_{ji}, given by

$$n_{ji} = N_{ji}(a_i b_{ji}) \qquad \text{for } i, j = 1, 2, 3. \tag{A1}$$

Three such outputs are summed per channel to provide factors m_j:

$$m_j = \sum_{i=1}^{3} n_{ji} = \sum_{i=1}^{3} N_{ji}(a_i b_{ji}) \qquad \text{for } j = 1, 2, 3. \tag{A2}$$

The form of the saturating nonlinearity that we use to fit the data of Fig. 7 is illustrated in Fig. 9 by the middle curve, labeled Medium. We generate this curve by splicing together a straight line and a doubly exponential function. For input values $a_i b_{ji}$ that are less than or equal to a constant c_{ji}, the nonlinearity N_{ji} simply equates the output with the input. For input values that exceed the constant c_{ji}, the nonlinearity has a doubly exponential form and is scaled to saturate at a maximum value $r_{\max,ji}$. For $i, j = 1, 2, 3$,

$$\begin{aligned} n_{ji} &= N_{ji}(a_i b_{ji}) = a_i b_{ji} && \text{for } a_i b_{ji} \le c_{ji}, \\ n_{ji} &= c_{ji} + (r_{\max,ji} - c_{ji}) \\ &\times \left(1 - \exp\left\{-\frac{[\exp(a_i b_{ji} - c_{ji}) - 1]}{(r_{\max,ji} - c_{ji})}\right\}\right) && \text{for } a_i b_{ji} > c_{ji}. \end{aligned} \tag{A3}$$

This nonlinearity of Eqs. (A3) has three valuable properties. This first is that, for small and moderate input values, the output is identical to the input: $n_{ji} = a_i b_{ji}$ for small a_i, i, $j = 1, 2, 3$. We want the output to be identical to the input for small and moderate inputs, so that the bilinear model matrix entries correspond to slopes found with small-to-moderate contrast stimuli in the linear range. An initial slope other than one for the nonlinearity would break this correspondence.

The second property of the nonlinearity is its saturation: for large input values the output is essentially identical to a constant, maximum response level $r_{\max,ji}$ for i, $j = 1, 2, 3$.

The third property of the nonlinearity is illustrated in Fig. 9. The curve marked Medium pictures the nonlinearity of Eqs. (A3) for values $c_{ji} = (1/2)$ and $r_{\max,ji} = 1$. The nonlinearity is neither a soft saturating nonlinearity like the exponential $1 - \exp(-t)$ (thin solid curve) nor a hard saturating nonlinearity like that indicated by the dashed-line segments. The nonlinearity is intermediate in degree, and one can vary it by changing the parameter c_{ji}. Specifically, the nonlinearity varies between the moderate doubly exponential one and the hard one by variation of c_{ji} between 0 and $r_{\max,ji}$, respectively.

We fitted the data in Fig. 7 by varying the nine bilinear model parameters b_{ji} and the two saturating nonlinearity parameters c and $r_{\max}$ for each of nine panels, so using a total of 27 parameters to fit 45 data points. Each null $\boldsymbol{\nu}$ measured at a particular annulus mean contrast $\mathbf{a}_m$, at a fixed annulus contrast modulation $\boldsymbol{\alpha}$ and at a fixed disk mean contrast $\mathbf{d}$, is given [see Eq. (12)] by

$$\begin{aligned}\boldsymbol{\nu}(\mathbf{a}_m, \boldsymbol{\alpha}) &= \mathbf{d}'(\mathbf{a}_m) - \mathbf{d}'(\mathbf{a}_m + \boldsymbol{\alpha}) \\ &= (\mathbf{I} - \mathbf{M}(\mathbf{a}_m))\mathbf{d} - [\mathbf{I} - \mathbf{M}(\mathbf{a}_m + \boldsymbol{\alpha})]\mathbf{d} \\ &= \mathbf{M}(\mathbf{a}_m + \boldsymbol{\alpha})\mathbf{d} - \mathbf{M}(\mathbf{a}_m)\mathbf{d} \\ &= \left\{ \begin{bmatrix} m_1(\mathbf{a}_m + \boldsymbol{\alpha}) & 0 & 0 \\ 0 & m_2(\mathbf{a}_m + \boldsymbol{\alpha}) & 0 \\ 0 & 0 & m_3(\mathbf{a}_m + \boldsymbol{\alpha}) \end{bmatrix} \right. \\ &\quad \left. - \begin{bmatrix} m_1(\mathbf{a}_m) & 0 & 0 \\ 0 & m_2(\mathbf{a}_m) & 0 \\ 0 & 0 & m_3(\mathbf{a}_m) \end{bmatrix} \right\} \mathbf{d}, \qquad \text{(A4)}\end{aligned}$$

in which functions m_1, m_2, and m_3 incorporate the saturating nonlinearities as per Eq. (A2) and the disk contrast $\mathbf{d}$ is known. We used the computer program `praxis`[41] to fit the data of Fig. 7.

ACKNOWLEDGMENTS

We thank Al Ahumada, Carol Cicerone, Dave Heeger, Geoffrey Iverson, and George Sperling for helpful discussions and Geoffrey Iverson for reading an earlier version of this manuscript. We thank Jennifer Chang, Lam Dinh, John Higgins, and Jason Lewis for their help with the experiments. This research was supported by National Eye Institute grant EY10014 to M. D'Zmura and by National Science Foundation grant DIR-9014278 to the Institute for Mathematical Behavioral Sciences, University of California, Irvine, R. D. Luce, director.

REFERENCES

1. A. Kirschmann, "Ueber die quantitativen Verhältnisse des simultanen Helligkeits- und Farben-Contrastes," Philos. Studien **6,** 391–417 (1890).
2. D. Jameson and L. M. Hurvich, "Opponent chromatic induction: experimental evaluation and theoretical account," J. Opt. Soc. Am. **51,** 46–53 (1961).
3. B. Singer and M. D'Zmura, "Color contrast induction," Vision Res. **34,** 3111–3126 (1994).
4. E. H. Land, "Recent advances in retinex theory and some implications for cortical computations: color vision and the natural image," Proc. Natl. Acad. Sci. (USA) **80,** 5163–5169 (1983).
5. J. J. McCann, "The role of simple nonlinear operations in modelling human lightness and color sensations," in *Human Vision, Visual Processing and Digital Display,* B. E. Rogowitz, ed., Proc. Soc. Photo-Opt. Instrum. Eng. **1077,** 355–363 (1989).
6. R. O. Brown and D. I. A. MacLeod, "Saturation and color constancy," in *Advances in Color Vision,* Vol. 4 of 1992 OSA Technical Digest Series (Optical Society of America, Washington, D.C., 1992), pp. 110–111.
7. K.-H. Bäuml, "Color appearance: the effect of illuminant changes on different surface collections," J. Opt. Soc. Am. A **11,** 531–542 (1994).
8. J. W. Jenness and S. K. Shevell, "Color appearance with sparse chromatic context," Vision Res. (to be published).
9. C. Chubb, G. Sperling, and J. A. Solomon, "Texture interactions determine perceived contrast," Proc. Natl. Acad. Sci. (USA) **86,** 9631–9635 (1989).
10. V. C. Smith and J. Pokorny, "Spectral sensitivity of the foveal cone photopigments between 400 and 500 nm," Vision Res. **15,** 161–171 (1975).
11. D. I. A. MacLeod and R. M. Boynton, "Chromaticity diagram showing cone excitation by stimuli of equal luminance," J. Opt. Soc. Am. **69,** 1183–1186 (1979).
12. J. Krauskopf, D. R. Williams, and D. M. Heeley, "The cardinal directions of color space," Vision Res. **22,** 1123–1131 (1982).
13. J. Krauskopf, Q. Zaidi, and M. B. Mandler, "Mechanisms of simultaneous color induction," J. Opt. Soc. Am. A **3,** 1752–1757 (1986).
14. J. A. Solomon, G. Sperling, and C. Chubb, "The lateral inhibition of perceived contrast is indifferent to on-center/off-center segregation, but specific to orientation," Vision Res. **33,** 2671–2683 (1993).
15. M. A. Webster and J. D. Mollon, "Changes in colour appearance following post-receptoral adaptation," Nature (London) **349,** 235–238 (1991).
16. M. A. Webster and J. D. Mollon, "The influence of contrast adaptation on colour appearance," Vision Res. **34,** 1993–2020 (1994).
17. M. W. Cannon and S. C. Fullenkamp, "Spatial interactions in apparent contrast: inhibitory effects among grating patterns of different spatial frequencies, spatial positions and orientations," Vision Res. **31,** 1985–1998 (1991).
18. D. H. Brainard and B. A. Wandell, "A bilinear model of the illuminant's effect on color appearance," in *Computational Models of Visual Processing,* M. S. Landy and J. A. Movshon, eds. (MIT Press, Cambridge, Mass., 1991), pp. 171–186.
19. C. M. Cicerone, D. H. Krantz, and J. Larimer, "Opponent-process additivity—III. Effect of moderate chromatic adaptation," Vision Res. **15,** 1125–1135 (1975).
20. J. Wei and S. K. Shevell, "Color appearance under chromatic adaptation varied along theoretically significant directions in color space," J. Opt. Soc. Am. A **12,** 36–46 (1995).
21. D. H. Marimont and B. A. Wandell, "Linear models of surface and illuminant spectra," J. Opt. Soc. Am. A **9,** 1905–1913 (1992).
22. M. D'Zmura, "Color constancy: surface color from changing illumination," J. Opt. Soc. Am. A **9,** 490–493 (1992).
23. M. D'Zmura and G. Iverson, "Color constancy. I. Basic theory of two-stage linear recovery of spectral descriptions for lights and surfaces," J. Opt. Soc. Am. A **10,** 2148–2165 (1993).

24. M. D'Zmura and G. Iverson, "Color constancy. II. Results for two-stage linear recovery of spectral descriptions for lights and surfaces," J. Opt. Soc. Am. A **10,** 2166–2180 (1993).
25. M. D'Zmura and G. Iverson, "Color constancy. III. General linear recovery of spectral descriptions for lights and surfaces," J. Opt. Soc. Am. A **11,** 2389–2400 (1994).
26. G. Sperling, "Three stages and two systems of visual processing," Spatial Vision **4,** 183–207 (1989).
27. D. J. Heeger, "Normalization of cell responses in cat striate cortex," Visual Neurosci. **9,** 181–197 (1992).
28. B. Singer, M. D'Zmura, G. Iverson, D. J. Lewis, and L. Dinh, "A bilinear model for color contrast induction," Invest. Ophthalmol. Vis. Sci. Suppl. **35,** 1656 (1994).
29. A. M. Derrington, J. Krauskopf, and P. Lennie, "Chromatic mechanisms in lateral geniculate nucleus of macaque," J. Physiol. (London) **357,** 241–265 (1984).
30. S. Ishihara, *The Series of Plates Designed as a Test for Colour-Blindness* (Kanehara, Tokyo, 1986).
31. W. H. Greub, *Multilinear Algebra* (Springer, New York, 1967).
32. J. von Kries, "Influence of adaptation on the effects produced by luminous stimuli," in *Handbuch der Physiologie de Menschen* (1905), Vol. 3, pp. 109–282; in *Sources of Color Vision,* D. L. MacAdam, ed. (MIT Press, Cambridge, Mass., 1970).
33. M. D'Zmura, "Color in visual search," Vision Res. **31,** 951–966 (1991).
34. J. Krauskopf, D. R. Williams, M. B. Mandler, and A. M. Brown, "Higher-order color mechanisms," Vision Res. **26,** 23–32 (1986).
35. M. D'Zmura and P. Lennie, "Mechanisms of color constancy," J. Opt. Soc. Am. A **3,** 1662–1672 (1986).
36. P. Lennie, J. Krauskopf, and G. Sclar, "Chromatic mechanisms in striate cortex of macaque," J. Neurosci. **10,** 649–669 (1990).
37. J. J. Atick, Z. Li, and A. N. Redlich, "What does post-adaptation color appearance reveal about cortical color processing?" Vision Res. **33,** 123–129 (1993).
38. Q. Zaidi and A. G. Shapiro, "Adaptive orthogonalization of opponent-color signals," Biol. Cybern. **69,** 415–428 (1993).
39. J. G. Robson, "Linear and non-linear operations in the visual system," Invest. Ophthalmol. Vis. Sci. Suppl. **29,** 117 (1988).
40. M. D'Zmura, B. Singer, L. Din, J. Kim, and J. Lewis, "Spatial sensitivity of contrast induction mechanisms," Opt. Photon. News **5,** Suppl. 48 (1994).
41. K. R. Gegenfurtner, "PRAXIS: Brent's algorithm for function minimization," Behav. Res. Meth. Instrum. Comput. **24,** 560–564 (1993).